Multiphase Evolution and Variational Image Classification

Christophe Samson, Laure Blanc-Féraud, Gilles Aubert, Josiane Zerubia

INRIA

INSTITUT NATIONAL DE RECHERCHE EN INFORMATIQUE ET EN AUTOMATIQUE

Multiphase Evolution and Variational Image Classification

Christophe Samson — Laure Blanc-Féraud — Gilles Aubert — Josiane Zerubia

N° 3662

Avril 1999

THÈME 3

ISSN 0249-6399

Multiphase Evolution and Variational Image Classification

Christophe Samson, Laure Blanc-Féraud, Gilles Aubert*, Josiane Zerubia

Thème 3 — Interaction homme-machine,
images, données, connaissances
Projet Ariana

Rapport de recherche n° 3662 — Avril 1999 — 42 pages

Abstract: This report presents a supervised classification model based on a variational approach. This model is devoted to find an optimal partition compound of homogeneous classes with regular interfaces. We represent the regions of the image defined by the classes and their interfaces by level set functions, and we define a functional whose minimum is an optimal partition. The coupled Partial Differential Equations (PDE) related to the minimization of the functional are considered through a dynamical scheme. Given an initial interface set (zero level set), the different terms of the PDE's are governing the motion of interfaces such that, at convergence, we get an optimal partition as defined above. Each interface is guided by internal forces (regularity of the interface), and external ones (data term, no vacuum, no regions overlapping). We conducted several experiments on both synthetic an real images.

Key-words: Variational model, classification, labelling, level set formulation, active regions, active contours, multiphase, satellite images.

* Laboratoire J.A. dieudonné UMR 6621 CNRS, Université de Nice-Sophia Antipolis, 06108 Nice Cedex 2, FRANCE

Unité de recherche INRIA Sophia Antipolis
2004, route des Lucioles, B.P. 93, 06902 Sophia Antipolis Cedex (France)
Téléphone : 04 92 38 77 77 - International : +33 4 92 38 77 77 —Fax : 04 92 38 77 65 - International : +33 4 92 38 77 65

Evolution de Phases Multiples et Classification d'Images par modèle variationnel

Résumé : Dans ce rapport, nous présentons un modèle de classification supervisée basé sur une approche variationnelle. Nous souhaitons obtenir une partition optimale de l'image constituée de classes homogènes séparées par des interfaces régulières. Pour cela, nous représentons les régions définies par les classes ainsi que leurs interfaces par des fonctions d'ensembles de niveaux. Nous définissons une fonctionnelle sur ces ensembles de niveaux dont le minimum est une partition optimale. Les Equations aux Dérivées Partielles (EDP) relatives à la minimisation de la fonctionnelle sont couplées et plongées dans une schéma dynamique. En fixant un ensemble de niveaux initial, les différents termes des EDP guident l'évolution des interfaces (ensembles de niveaux zéro) vers les frontières de la partition optimale, par le biais de forces internes (régularité de l'interface) et externes (attache aux données et pas de chevauchement des régions ni de vide dans la partition). Nous avons effectué de nombreux tests sur des images synthétiques ainsi que sur des images réelles.

Mots-clés : Modèle variationnel, classification d'images, formulation par ensembles de niveaux, régions actives, contours actifs, phases multiples, images satellitaires.

Contents

1 Introduction

Image classification, which consists of assigning a label to each pixel of an observed image, is one of the basic problems in image processing. This concerns many applications as, for instance, land use management in teledetection. The classification problem is closely related to the segmentation one, in the sense that we want to get a partition compound of homogeneous regions. Nevertheless, within the classification procedure, each partition represents a class, i.e. a set of pixels with the same label. In the following, the feature criterion we are interested in is the spatial distribution of intensity (or grey level). This work takes place in the general framework of supervised classification which means that the number and the parameters of the classes are known. The proposed method could be extended to other discriminant features than grey-level such as texture for instance. The unsupervised case, including a parameter estimation capability, will be studied in the future.

Many classification models have been developed with structural notions as region growing methods for example [20], or by stochastic approach as in [2, 3, 7, 8, 13, 15, 17], but rarely in the field of variational approach. In [22, 23] we proposed a supervised variational classification model based on Cahn-Hilliard models, such that the solution we get is compound of homogeneous regions separated by regularized boundaries. The classes are considered as phases separated by interfaces boundaries. The model was developed through considerations of regularity on the phases by defining a set of functionals whose expected minimum at convergence is an image with expected properties of regularity.
Herein, the approach is different, mainly because the proposed model is based on active contours, and the functional of interest is defined over the regions with associated interfaces through a level set model. The resulting dynamical Partial Differential Equations (PDE's), governing the evolution of the set of interfaces, consist of a moving front converging to a regularized partition. This model is inspired by the work of Zhao et *al.* about multiphase evolution [25], and takes place in the general framework of active contours [4, 5, 12, 16] for region segmentation [19, 21, 26]. We use a level set formulation [18] which is convenient to write functional depending on regions and contours, and allows a change of topology of the evolving fronts. Each active interface is coupled to the other ones through a term which penalizes overlapping regions (i.e. pixels with two labels) and the formation of vacuum (i.e. pixels without any label). The evolution of each interface is guided by forces that impose the following constraints : the interface exhibits a minimal perimeter (internal force) and it encloses one and only one homogeneous class (external force).

First, we state the problem of classification as a partitioning problem. We clearly set the framework and define the properties we expect on the classification. Second, we expose the classification statement through a level set formulation. The Euler-Lagrange derivative of the proposed functional leads to a dynamical scheme we propose to implement. We then propose to introduce a restoration process in the model which permits to deal with degradated data. We finally present some experimental results on both synthetic and real images, and also on noisy data.

2 Image classification as a partitioning problem

This section is devoted to present the properties we want the classification model to satisfy. In the following, we consider a classification problem in which a partition of the observed data u_0, with respect to the predefined classes, is searched. This partition is compound of homogeneous regions, say the classes, separated by regularized interfaces. Herein, we suppose that the classes have a Gaussian distribution of intensity, therefore a class is characterized by its mean μ_i and its standard deviation σ_i. The number K of classes and the parameters $(\mu_i;\sigma_i)_{i=1...K}$ are supposed to be given from a previous estimation. We choose to assign the label value μ_i to each element of the i$^{\text{th}}$ class. All indexes i or j are going from 1 to K.

Let Ω be an open domain subset of $\mathbb{R}^2$ with smooth boundary, and let $u_0 : \Omega \to \mathbb{R}$ represent the observed data function. Let Ω_i be the region defined as

$$\Omega_i = \{x \in \Omega / x \text{ belongs to the i}^{th} \text{ class}\}. \tag{1}$$

A partitioning of Ω consists of finding a set $\{\Omega_i\}_{i=1...K}$ such that (see Fig. 1)

$$\Omega = \bigcup_{i=1}^{K} \Omega_i \quad \text{and} \quad \Omega_i \bigcap_{i \neq j} \Omega_j = \varnothing. \tag{2}$$

We note $\Gamma_i = \partial\Omega_i \cap \Omega$ the boundary of region Ω_i (excepted the common points with $\partial\Omega$), and let the interface between Ω_i and Ω_j be

$$\Gamma_{ij} = \Gamma_{ji} = \Gamma_i \cap \Gamma_j \cap \Omega, \quad \forall i \neq j. \tag{3}$$

We have

$$\Gamma_i = \bigcup_{j \neq i} \Gamma_{ij}. \tag{4}$$

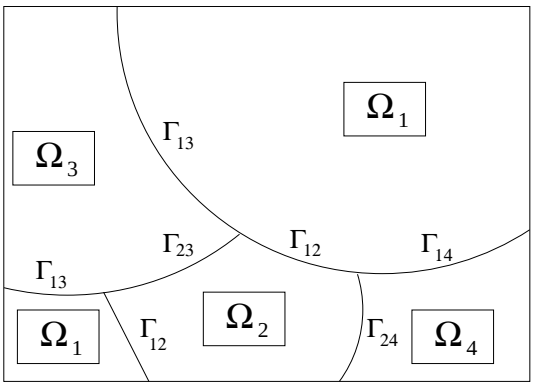

Figure 1: A partition of Ω.

Let remark that in (3) and (4) we eventually have $\Gamma_{ij} = \varnothing$. We note $|\Gamma_i|$ the one-dimensional Hausdorff measure of Γ_i verifying

$$|\Gamma_i| = \sum_{j \neq i} |\Gamma_{ij}| \text{ and } |\varnothing| = 0. \tag{5}$$

The classification model we consider for an image u_o defined over Ω, is a set $\{\Omega_i\}_i$ defined by (1) and satisfying :

Condition a : $\{\Omega_i\}_i$ is a partition of Ω :

$$\Omega = \bigcup_i \Omega_i \quad \text{and} \quad \Omega_i \bigcap_{i \neq j} \Omega_j = \varnothing.$$

Condition b : The partition $\{\Omega_i\}_i$ is a classification of the observed data u_0 and takes into account the Gaussian distribution property of the classes (data term) :

$$\text{minimize} \sum_i \int_{\Omega_i} \Big(\frac{u_0 - \mu_i}{\sigma_i} \Big)^2 \quad \text{with respect to } \Omega_i.$$

Condition c : The partition is regular in the sense that the sum of the length of interfaces Γ_{ij} is minimum :

$$\text{minimize} \sum_{i,j} \xi_{ij} |\Gamma_{ij}| \quad \text{with respect to } \Gamma_{ij} \quad (\xi_{ij} \in \mathbb{R} \text{ are fixed}).$$

The solution of the classification model proposed in the next section has to take into account the three conditions. This is done by associating a functional to the set of interfaces such that minimizers will respect CONDITIONS A, B and C.

3 Multiphase model : image classification in terms of level set

The classification model developed further is based on coupled active interfaces, and the approach we adopt is inspired from Zhao et *al.* [25]. The evolution of each interface is guided by forces constraining the solution to respect CONDITIONS A, B and C exposed in the previous section. We use a level set formulation to represent each interface and also each region Ω_i element of the partition $\{\Omega_i\}_i$.

3.1 Preliminaries

Let $\Phi_i : \Omega \times \mathbb{R}^+ \to \mathbb{R}$ be a Lipschitz function associated to region Ω_i (we assume the existence of such a Φ_i) such that

$$\begin{cases} \Phi_i(x;t) > 0 & \text{if } x \in \Omega_i \\ \Phi_i(x;t) = 0 & \text{if } x \in \Gamma_i \\ \Phi_i(x;t) < 0 & \text{otherwise .} \end{cases} \tag{6}$$

Thus, the region Ω_i is entirely described by the function Φ_i (see Fig. 3). In the following, for a sake of clarity, we will sometimes omit spatial parameter x and time parameter t in $\Phi_i(x;t)$.
Let define the approximations δ_α and H_α of Dirac and Heaviside distributions (cf. Fig. 2) with $\alpha \in \mathbb{R}^+$

$$\delta_\alpha(s) = \begin{cases} \frac{1}{2\alpha}\Big(1 + \cos(\frac{\pi s}{\alpha})\Big) & \text{if } |s| \leq \alpha \\ 0 & \text{if } |s| > \alpha \end{cases} \tag{7}$$

$$H_\alpha(s) = \begin{cases} \frac{1}{2}\Big(1 + \frac{s}{\alpha} + \frac{1}{\pi}\sin(\frac{\pi s}{\alpha})\Big) & \text{if } |s| \leq \alpha \\ 1 & \text{if } s > \alpha \\ 0 & \text{if } s < \alpha \end{cases} \tag{8}$$

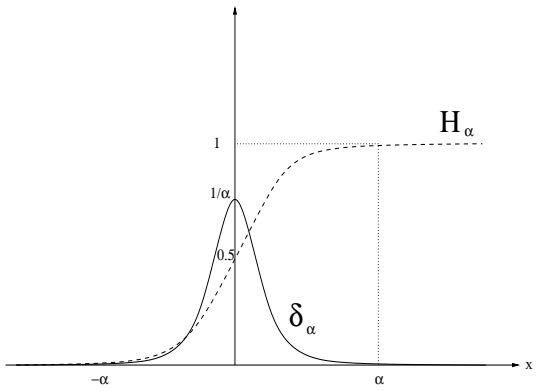

Figure 2: Approximations δ_α and H_α of Dirac and Heaviside distributions.

and we have

$$\begin{cases} \delta_\alpha \overset{\mathcal{D}'(\Omega)}{\longrightarrow} \delta & \text{as } \alpha \to 0^+ \\ H_\alpha \overset{\mathcal{D}'(\Omega)}{\longrightarrow} H & \text{as } \alpha \to 0^+ \end{cases}$$

where $\mathcal{D}'(\Omega)$ is the space of distributions defined over Ω. From (6),(7) and (8) we can write (see Fig. 3)

$$\{x \in \Omega / \lim_{\alpha \to 0^+} H_\alpha(\Phi_i(x;t)) = 1\} = \Omega_i \tag{9}$$

$$\{x \in \Omega / \lim_{\alpha \to 0^+} \delta_\alpha(\Phi_i(x;t)) \neq 0\} = \Gamma_i. \tag{10}$$

3.2 Multiphase functional

Let $u_0 : \Omega \to \mathbb{R}$ be the observed data (grey level for instance).

Thanks to the level set Φ_i's defined in (6) and by the use of (9) and (10), a partition $\{\Omega_i\}_i$ respecting CONDITIONS A, B and C stated in section 2 can be found through the minimization of a global functional depending on the Φ_i's. This functional contains three terms, each one being related to one of the three conditions. In the following, we express each condition in term of functional minimization. Minimizers of the

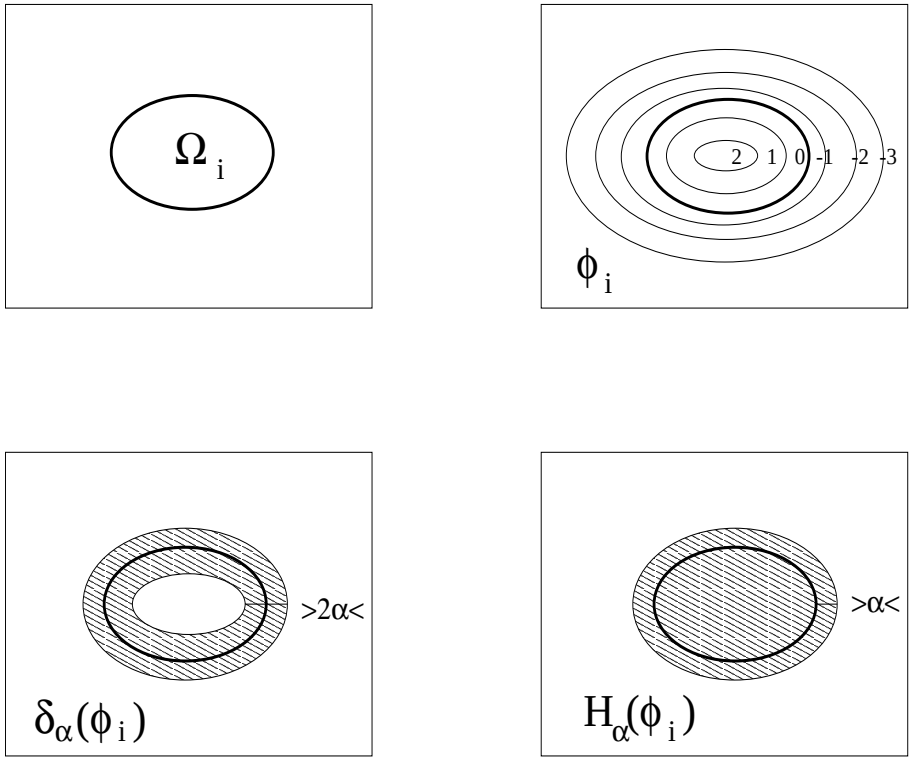

Figure 3: Illustration of the signed distance function Φ_i (top right handside) associated to region Ω_i (top left handside). Filled regions on both figures on bottom handside represent non-zero regions for $\delta_\alpha(\Phi_i)$ (on the left) and for $H_\alpha(\Phi_i)$ (on the right).

following functionals are supposed to exist.

• FUNCTIONAL RELATED TO CONDITION A (PARTITION CONDITION) :
Let define the following functional :

$$F_\alpha^{\mathrm{A}}(\Phi_1, ..., \Phi_K) = \frac{\lambda}{2} \int_\Omega \Big(\sum_{i=1}^{K} H_\alpha(\Phi_i) - 1 \Big)^2 dx \quad \text{with } \lambda \in \mathbb{R}^+ \ . \tag{11}$$

The minimization of F_α^{A}, as $\alpha \to 0^+$, penalizes the formation of vacuum (pixels with no label) and regions overlapping (pixels with more than one label).

• FUNCTIONAL RELATED TO CONDITION B (DATA TERM) :
Taking into account the observed data and the Gaussian distribution property of the classes, we consider :

$$F_\alpha^{\mathrm{B}}(\Phi_1, ..., \Phi_K) = \sum_{i=1}^{K} e_i \int_\Omega H_\alpha(\Phi_i) \frac{(u_o - \mu_i)^2}{\sigma_i^2} dx \quad \text{with } e_i \in \mathbb{R}, \forall i. \tag{12}$$

The family $\{\Phi\}_i$ minimizing F_α^{B} as $\alpha \to 0^+$ leads to a partition $\{\Omega_i\}_i$ satisfying CONDITION B.

• FUNCTIONAL RELATED TO CONDITION C (LENGTH SHORTENING OF INTERFACE SET) :
The last functional we want to introduce is related to CONDITION C about the minimization of the interfaces length. We would like to minimize

$$\frac{1}{2} \sum_{i,j} \xi_{ij} |\Gamma_{ij}| \quad \text{with } \xi_{ij} \text{ being real constants.} \tag{13}$$

The factor $\frac{1}{2}$ expresses the symmetry $\Gamma_{ij} = \Gamma_{ji}$ and will be introduced in the weighting parameters ξ_{ij}. We turn the minimization of interfaces length into the minimization of boundaries length :

$$\sum_{i=1}^{K} \gamma_i |\Gamma_i| \quad \text{with } \gamma_i \text{ being real constants.} \tag{14}$$

From (13) and (14) we obtain the constraint $\xi_{ij} = \gamma_i + \gamma_j$ which permits to select the weighting parameters γ_i in the problem of boundaries length minimization to retrieve

the interfaces length minimization one[1]. According to Lemma 1 exposed below, the minimization of (14) is operated by minimizing the functional (as $\alpha \to 0^+$) :

$$F_\alpha^C(\Phi_1, ..., \Phi_K) = \sum_{i=1}^{K} \gamma_i \int_\Omega \delta_\alpha(\Phi_i)|\nabla\Phi_i|dx. \tag{15}$$

Let recall the Coarea formula :

Theorem 1 (Coarea formula [9]) *Let $f : \mathbb{R}^2 \to \mathbb{R}$ be a Lipschitz function and $g \in L^1(\mathbb{R}^2)$, then :*

$$\int_{\mathbb{R}^2} g(x)|\nabla f(x)|dx = \int_{\mathbb{R}} \Big[\int_{f=\rho} g(x)ds\Big] d\rho$$

Then, from the Coarea formula we get :

Lemma 1 *According to the previous definitions, let define*

$$L_\alpha(\Phi_i) = \int_\Omega \delta_\alpha(\Phi_i(x;t))|\nabla\Phi_i(x;t)|dx,$$

then we have

$$\lim_{\alpha\to 0} L_\alpha(\Phi_i) = \int_{\Phi_i=0} ds = |\Gamma_i|.$$

Proof : in the Coarea formula, we choose $g(x) = \delta_\alpha(\Phi_i(x;t))$ and $f(x) = \Phi_i(x;t)$, then we have

$$\begin{aligned} L_\alpha(\Phi_i) &= \int_{\mathbb{R}} \Big[\int_{\Phi_i=\rho} \delta_\alpha(\Phi_i(x;t))ds\Big] d\rho \\ &= \int_{\mathbb{R}} \Big[\delta_\alpha(\rho) \int_{\Phi_i=\rho} ds\Big] d\rho \end{aligned}$$

By setting $h(\rho) = \int_{\Phi_i=\rho} ds$ we obtain

$$\begin{aligned} L_\alpha(\Phi_i) &= \int_{\mathbb{R}} \delta_\alpha(\rho)h(\rho)d\rho \\ &\overset{(7)}{=} \frac{1}{2\alpha}\int_{-\alpha}^{\alpha} \Big(1 + \cos(\frac{\pi\rho}{\alpha})\Big)h(\rho)d\rho \end{aligned}$$

[1] $\sum_{i,j\neq i} \xi_{ij}|\Gamma_{ij}| = \sum_i \gamma_i|\Gamma_i| \overset{(4)}{=} \sum_i \gamma_i|\cup_{j\neq i}\Gamma_{ij}| = \sum_i \gamma_i \sum_{j\neq i}|\Gamma_{ij}| = \sum_{i,j\neq i}(\gamma_i + \gamma_j)|\Gamma_{ij}|$

If we take $\theta = \frac{\rho}{\alpha}$ we have

$$L_\alpha(\Phi_i) = \frac{1}{2}\int_{-1}^{1}\Big(1+\cos(\pi\theta)\Big)h(\alpha\theta)d\theta$$

Thus, when $\alpha \to 0$ we obtain

$$\begin{aligned}\lim_{\alpha\to 0} L_\alpha(\Phi_i) &= \frac{1}{2}h(0)\int_{-1}^{1}\Big(1+\cos(\pi\theta)\Big)d\theta \\ &= h(0) = \int_{\Phi_i=0} ds = |\Gamma_i|\end{aligned}$$

———

• GLOBAL FUNCTIONAL :
The sum $F_\alpha^{\mathrm{A}} + F_\alpha^{\mathrm{B}} + F_\alpha^{\mathrm{C}}$ leads to the global functional :

$$\begin{aligned}F_\alpha(\Phi_1,...,\Phi_K) = \sum_{i=1}^{K} e_i \int_\Omega H_\alpha(\Phi_i)\frac{(u_o-\mu_i)^2}{\sigma_i^2}dx + \sum_{i=1}^{K}\gamma_i\int_\Omega \delta_\alpha(\Phi_i)|\nabla\Phi_i|dx \\ +\frac{\lambda}{2}\int_\Omega\Big(\sum_{i=1}^{K}H_\alpha(\Phi_i)-1\Big)^2dx \qquad (16)\end{aligned}$$

As $\alpha \to 0^+$, the solution set $\{\Phi_i\}_i$ minimizing $F_\alpha(\Phi_1,...,\Phi_K)$, if it exists[2] and according to (6), defines a classification compound of homogeneous classes (the so-called Ω_i *phases*) separated by regularized interfaces.

3.3 Remark about length minimization

Consider the length functional :

$$L(t) = \int_0^1 |\frac{\partial C(p;t)}{\partial t}|dt \qquad (17)$$

where $\{C(p;t)\}_t$ is a set of closed parametrized ($p \in [0;1]$) curves over Ω such that $C(0;t) = C(1;t)$ and $\frac{\partial C(0;t)}{\partial t} = \frac{\partial C(1;t)}{\partial t}$. Then, $L(t)$ is decreasing most rapidly if

$$\frac{\partial C(p;t)}{\partial t} = \kappa\vec{N} \qquad (18)$$

[2]If they exist, minimizers $\{\Phi_i\}_i$ should be found in the space $\{\Phi_i : \Omega\times\mathbb{R}^+ \to \mathbb{R}/|\nabla\Phi_i| \in L^1(\Omega)\}$

κ being the local curvature of $C(p;t)$ and $\vec{N}$ the inward normal. Curve evolution through PDE (18) is known as *mean curvature motion* (see [14] for instance). Active contours guided by (18) tends to regular curves in the sense that the length is minimized. PDE (18) can be written through a level set formulation [18] which is more convenient to manage curves breaking and merging. Assume that $d : \Omega \times \mathbb{R}^+ \rightarrow \mathbb{R}$ is a smooth continuous function such that, from the value of $d(x;t)$, we can determine if x is interior, exterior or belongs to $C(p;t)$. Let suppose that : $C(p;t) = \{x \in \Omega / d(x;t) = a\}$ (i.e. the contour is represented by level set a of function d). PDE (18) formulated by the use of level set becomes

$$\frac{\partial d(x;t)}{\partial t} = div(\frac{\nabla d}{|\nabla d|})|\nabla d|, \tag{19}$$

with $div(\frac{\nabla d}{|\nabla d|})$ being the local curvature of level set a. Equation (19) was studied for instance in [1, 10]. Evolution of level sets of function d (and so evolution of contour $C(p;t)$ through level set a) from (19) is the level set formulation of mean curvature motion. The level set formulation allows breaking and merging fronts which is not possible from formulation (18). Since contour $C(p;t)$ is represented by level set a, we only need to update PDE (19) in a narrow band around a. In this case, the level set formulation (19) comes from a reformulation of (18) to track the motion of contours $C(p;t)$. In our case, we directly define a length functional F_α^c over contours Γ_i's by the use of level set Φ_i's. The associated Euler-Lagrange equations lead to K PDE's of the form

$$\frac{\partial \Phi_i(x;t)}{\partial t} = div(\frac{\nabla \Phi_i}{|\nabla \Phi_i|})\delta_\alpha(\Phi_i). \tag{20}$$

Compared to PDE (19), we get from (20) a "natural" narrow band from the Dirac operator δ_α whose width depends on the value of α (for Φ_i's defined as signed distance in (6)). Fig. 4 shows the zero level set evolution of the Φ_i's through PDE (20).

4 Multiphase evolution scheme

Herein describe the way we minimize F_α in (16) with respect to $\Phi_1, ..., \Phi_K$. We obtain a dynamical system of K coupled PDE's.

4.1 System of coupled PDE's

If $(\Phi_1, ..., \Phi_K)$ is solution of the minimization of F_α, then necessarily[3]

$$\frac{\partial F_\alpha}{\partial \Phi_i} = 0, \ \forall i = 1...K. \tag{21}$$

With Neumann conditions ($\frac{\partial \Phi_i}{\partial \vec{n}}(x;t) = 0, \forall x \in \partial\Omega$), the Euler Lagrange equations associated to F_α give (see Appendix for more details about the computation of derivatives) the K following coupled PDE's

$$\frac{\partial F_\alpha}{\partial \Phi_i} = \delta_\alpha(\Phi_i)\Big[e_i\frac{(u_0-\mu_i)^2}{\sigma_i^2} - \gamma_i div\Big(\frac{\nabla\Phi_i}{|\nabla\Phi_i|}\Big) + \lambda\Big(\sum_{i=1}^{K} H_\alpha(\Phi_i) - 1\Big)\Big] = 0, \quad i = 1...K \tag{22}$$

with div denoting the divergence operator, and $div\big(\frac{\nabla\Phi_i}{|\nabla\Phi_i|}\big)$ being the (mean) curvature of level set Φ_i at point x. We note that the term $\delta_\alpha(\Phi_i)$ in (22) delimits a "natural" band in which the i$^{\text{th}}$ PDE is non zero valued (for Φ_i's being signed distance functions) : $B_\alpha^i = \{x \in \Omega / |\Phi_i(x;t)| \leq \alpha\}$.

4.2 Algorithm

We embed (22) into a dynamical scheme, we get a system of K coupled equations $(i = 1...K)$:

$$\Phi_i^{t+1} = \Phi_i^t - dt\Big(\delta_\alpha(\Phi_i)\Big[e_i\frac{(u_0-\mu_i)^2}{\sigma_i^2} - \gamma_i div\Big(\frac{\nabla\Phi_i}{|\nabla\Phi_i|}\Big) + \lambda\Big(\sum_{i=1}^{K} H_\alpha(\Phi_i) - 1\Big)\Big]\Big), \tag{23}$$

where dt is the step in time.
Let Ω be a grid with N lines and M columns. The horizontal and vertical steps of discretization are set to 1. We select a small value for α. According to the chosen step of discretization and for Φ_i's such that $|\nabla\Phi_i| = 1$, as it is for signed distance functions, we can see from (7) that the band B_α^i contains $2\alpha - 1$ (if $\alpha \in \mathbb{N}$) pixels. We do not make α decrease to 0, but we directly set α to a small value (not too small in order to have enough pixels in B_α^i for the calculus of the different terms of (23)), and in our experiments $\alpha = 3.0$. Let remark that we initially set the Φ_i's to signed

[3] if the Φ's are regular enough

distance functions which is commonly used for level set schemes. But as for (19), PDE's (20) and (23) do not maintain the the constraint $|\nabla\Phi_i| = 1$, and we regularly need to regularize the level sets Φ_i to be sure they remain signed distance functions. This can be done for instance by the use of PDE [24]

$$\frac{\partial\Phi_i(x;t)}{\partial t} = sign(\Phi_i)(1 - |\nabla\Phi_i|), \tag{24}$$

sign being the function returning the sign of the argument.
Here is the algorithm resulting from (23)

0 - Fix Φ_i^0 for $i = 1...K$
1 - $t \leftarrow t + 1$
    2 - For $i = 1...K$ solve the K coupled PDE's (23)
    3 - each n iteration of (23), regularize the Φ_i's with PDE (24)
4 - go to **1**

Step 0 is the initialization of the Φ_i's. This initialization is very important. A bad initialization leads to a bad classification. The Φ_i^0's can be manually chosen, or can be automatically computed from an initial pre-segmentation process, or automatically selected from computed "seeds" (see next section). The algorithm is stopped when the evolution of the solution between two iterations with respect to t is not significant, or when a fixed maximum number of iterations is reached.

5 A way to include a restoration process

The observed data u_0 can be corrupted by different sources of degradation, usually modeled by the following linear degradation equation :

$$u_0(x) = Ru(x) + \eta \tag{25}$$

with $u : \Omega \to \mathbb{R}$ being the original non noisy data, R is the impulse response of the system, and η is an additive Gaussian noise. This noisy information can interfere with the classification process and may induce misclassified pixels. So, in addition to the partitioning capability, we want the model to remove degraded pixels without damaging the set of edges of the image which represent important features of data

u_0. Based on edge-preserving restoration [6], we introduce the following functional :

$$G_\alpha(u,\Phi_1,...,\Phi_K) = \sum_{i=1}^{K}\gamma_i\int_\Omega \delta_\alpha(\Phi_i)|\nabla\Phi_i|dx + \frac{\lambda_1}{2}\int_\Omega\Big(\sum_{i=1}^{K}H_\alpha(\Phi_i)-1\Big)^2dx$$
$$+\sum_{i=1}^{K}e_i\int_\Omega H_\alpha(\Phi_i)\frac{(u-\mu_i)^2}{\sigma_i^2}dx$$
$$+\Lambda\Big[\int_\Omega (Ru-u_o)^2 + \lambda_2\int_\Omega\varphi(|\nabla u|)\Big] \qquad (26)$$

Function $\varphi : \mathbb{R}\to\mathbb{R}^+$ is a regularizing function with at least the two following properties : $\varphi(t)$ has a quadratic behavior near $t=0$ (*smoothing* effect), and is linear or sub-linear for $t\sim\infty$ (*edge-preserving* effect). We can find some examples of regularizing functions in [6]. The parameter $\Lambda\in\mathbb{R}^+$ is weighting the restoration part of functional G_α. The minimization of G_α with respect to u leads to the edge-preserved restoration of u taking into account the informations given by the partition term (third term on the right handside of (26) that attracts the values of u towards the mean of the classes), and the minimizations of G_α with respect to the Φ_i's gives a partition of u_0. The Euler-Lagrange equations associated to the minimization of G_α are :

$$\frac{\partial G_\alpha}{\partial u} = \sum_{i=1}^{K}e_iH_\alpha(\Phi_i)\frac{(u-\mu_i)}{\sigma_i} + \Lambda\Big[R^*(Ru-u_o) - \lambda_2 div\Big(\frac{\varphi'(|\nabla u|)}{2|\nabla u|}\nabla u\Big)\Big] = 0, \quad (27)$$

with R^* being the conjugate of R, and for $i=1...K$ we have

$$\frac{\partial G_\alpha}{\partial\Phi_i} = \delta_\alpha(\Phi_i)\Big[e_i\frac{(u-\mu_i)^2}{\sigma_i^2} - \gamma_i div\Big(\frac{\nabla\Phi_i}{|\nabla\Phi_i|}\Big) + \lambda_1\Big(\sum_{i=1}^{K}H_\alpha(\Phi_i)-1\Big)\Big] = 0. \qquad (28)$$

We alternate resolutions of (27) and (28) until the solution set $(u,\Phi_1,...,\Phi_K)$ does not evolve anymore. The resolution of (27) is done thanks to the half-quadratic regularization method [6, 11] based on the introduction of an auxiliary variable related to the discontinuity set. System (28) is embeded in a dynamical scheme as for the resolution of (22) with the dynamical system (23).

6 Experimental results

We made some experiments on both synthetic and real images. Some of the noisy data have been corrupted by an additive Gaussian noise. The Gaussian parameters

of the classes μ_i and σ_i $(i = 1...K)$ are supposed to be known from a previous estimation for instance. For all the results shown hereafter, we fix $\alpha = 3.0$. All initial Φ_i's are set to signed distance functions.

In the following, **ZLS** will stand for "zero level set" of functions Φ_i's, and **Phase image** represents the map of the K regions surrounded by the ZLS's, whose grey level values are set to the mean values μ_i.

6.1 Synthetic images

6.1.1 Non noisy data

On Fig. 4 we show the motion of the ZLS's of functions Φ_i's through PDE (20), i.e. parameters λ and e_i are set to zero for all i in (23). This evolution reflects the influence of length shortening term F_α^C defined in (15). We have initialized three circular and overlapping signed distance functions. Fig. 4 presents the motion of the ZLS's : three circles with initially same radius. We remark that the evolution of circular level sets through (20) leads to results of same type than classical mean curvature motion by level set approach defined in (19) : the ZLS's remain smooth circles whose radii are decreasing, and they finally shrink after iteration 800 for our experiment.

From Fig. 5 to Fig. 20, the initial Φ_i's are circular signed distance functions, and we present both evolution of Φ_i ZLS's and what we call "phase evolution", i.e. the motion of regions surrounded by the ZLS's. When not mentioned, the values of σ_i are equal to 1.0.

On Fig. 5 and Fig. 6, we give a result for three classes whose boundaries constitute a "T-junction". The initial overlapping and vacuum regions are vanishing thanks to the term F_α^A and the regularity of the level sets Φ_i's is obtained from F_α^C. We see that the interface between class 2 and class 1 is found later than the one between class 3 and class 1, because of the data term : the transition value between class 3 ($\mu_3 = 3.0$) and class 1 ($\mu_1 = 1.0$) is higher than the one between class 2 ($\mu_2 = 2.0$) and class 1.
We expose on Fig. 7 and Fig. 8 results for three classes of different shape and different curvature. We choose a small value for the γ_i's in order to retrieve the non smooth boundary of the class 3 object on the right handside.
Results on Fig. 9 and Fig. 10 reveal the behavior of the model when we start with

a "bad" initialization. Initial ZLS's for class 2 and class 3 are not judiciously set (see initial ZLS's on Fig. 9). We remark that from iteration 50 to iteration 150, the ZLS of Φ_2 is cut in two curves, the left one being constituted with only few pixels over the left part of class 2. This tiny seed is sufficient to detect the boundary of the left part of class 2. This phenomena shows that, even if the evolution of the ZLS's depends on the initialization set $\{\Phi_i^0\}_i$, we have a certain tolerance for the choice of initial sets.

6.1.2 Noisy data

The data on Fig. 11 and Fig. 12 are a noisy version of data treated on Fig. 5. A Gaussian noise has been added to the orignal data and the signal to noise ratio (SNR) in variances reaches -1.6 dB (Fig. 11) and -6.4 dB (Fig. 12). The variance parameters σ_i^2 are set to the value of the Gaussian noise. The initialization is the same than for the non noisy case, but parameters are different. Due to noisy pixels, the data term is low valued. To avoid the detection of isolated pixels, the value of the length shortening term has to be much more important than the data term (this leads to a quite wide vaccum region around the T-junction on Fig. 12, but we prefered to avoid the detection of noisy pixels, which are false alarm, than recovering non classified pixels). If we do not choose a high value for λ, the evolution of the zero level sets can prematurely stop. We present on Fig. 13 a comparison between the model without restoration terms (i.e the minimization of (16)) and with restoration term (i.e the minimization of (26) for $R = Id$) for noisy data exposed on (Fig. 12). We remark that the restoration capability of the model expressed through (26) leads to a classification result containing less vacuum, and less perturbated boundaries.
Data on Fig. 14 and Fig. 17 are a noisy version of data treated on Fig. 7. A Gaussian noise has been added to the orignal data and the SNR is equal to 3.2 dB. We choose the same initialization as for the non noisy case of Fig. 7. We note that the classification contains a lot of unclassified pixels on interfaces set (black pixels on false color image on Fig. 14), and also on homogeneous regions (see the two small isolated regions on the ZLS's final result). This kind of initialization, in the case of noisy data, is quite sensitive to noisy pixels because each ZLS sweeps over a wide region of the noisy data. We see on these results that we can not choose a set of parameters leading to smaller vacuum regions at the risk of being more sensitive to isolated pixels. That is the reason why we performed another initialization procedure, which is automatic and less sensitive to noise in the sense that the initial Φ_i's are sweeping over a wideless region of the noisy data.

For the following results, we use an automatic initialization we will call **seed initialization**. This method consists of cutting the data image of u_0 into N windows $W_{l,\,l=1..N}$ of predefined size. We compute the average m_l of u_0 on each window W_l. We then select the index k such that $k = arg\,\min_j (m_l - \mu_j)^2$. And we initialize the corresponding circular signed distance function Φ_k on each W_l. Windows are not overlapping and each of them is supporting one and only one function Φ_k, therefore we avoid overlapping of initial Φ_k's. The size of the windows is related to the smallest details we expect to detect. The major avantages of this simple initialization method are : it is automatic (only the size of the windows has to be fixed), it accelerates the speed of convergence (the smaller the windows, the faster the convergence), and it is less sensitive to noise (in the sense that we compute the average m_l of u_0 over each window before selecting the function Φ_k whose mean μ_k is the closest one to m_l).

The data on Fig. 16 and Fig. 17 are the same noisy data treated as the ones shown on Fig. 14, but we use an automatic seed initialization whose windows are of size 5×5. The size of the windows are small in order to avoid a lost of many details on the boundary of the perturbated shape on the right handside. The initial seeds are growing until they merge. Results are better than the ones obtained with the initialization set of Fig. 14.

6.2 Real images

Orignal data on Fig. 18 are MRI medical brain data containing 4 classes of pre-estimated parameters μ_i and σ_i. We present a color classification result and three steps of the ZLS and phase evolution obtained with an automatic seed initalization (on windows of size 5×5).

Data on Fig 19 and Fig 20 are SPOT satellite images provided by the French Space Agency CNES. Fig 19 contains 4 classes whose parameters were estimated in [2], and we have 10 classes for Fig 20 whose parameters were given by an expert (see [13]).

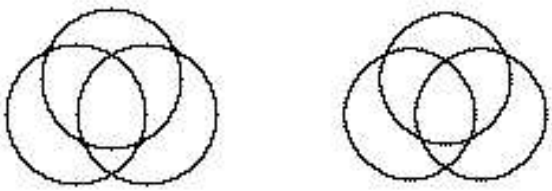

initialization iteration 100

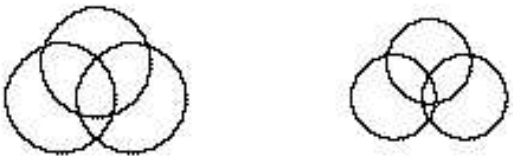

iteration 300 iteration 500

iteration 700 iteration 800

Figure 4: Evolution of the three ZLS's. Parameters λ and e_i in (23) are set to zero for all $i = 1...K$. Only the length shortening term is taken into account : $\gamma_i = 10.0\ \forall i$, and $dt = 0.2$

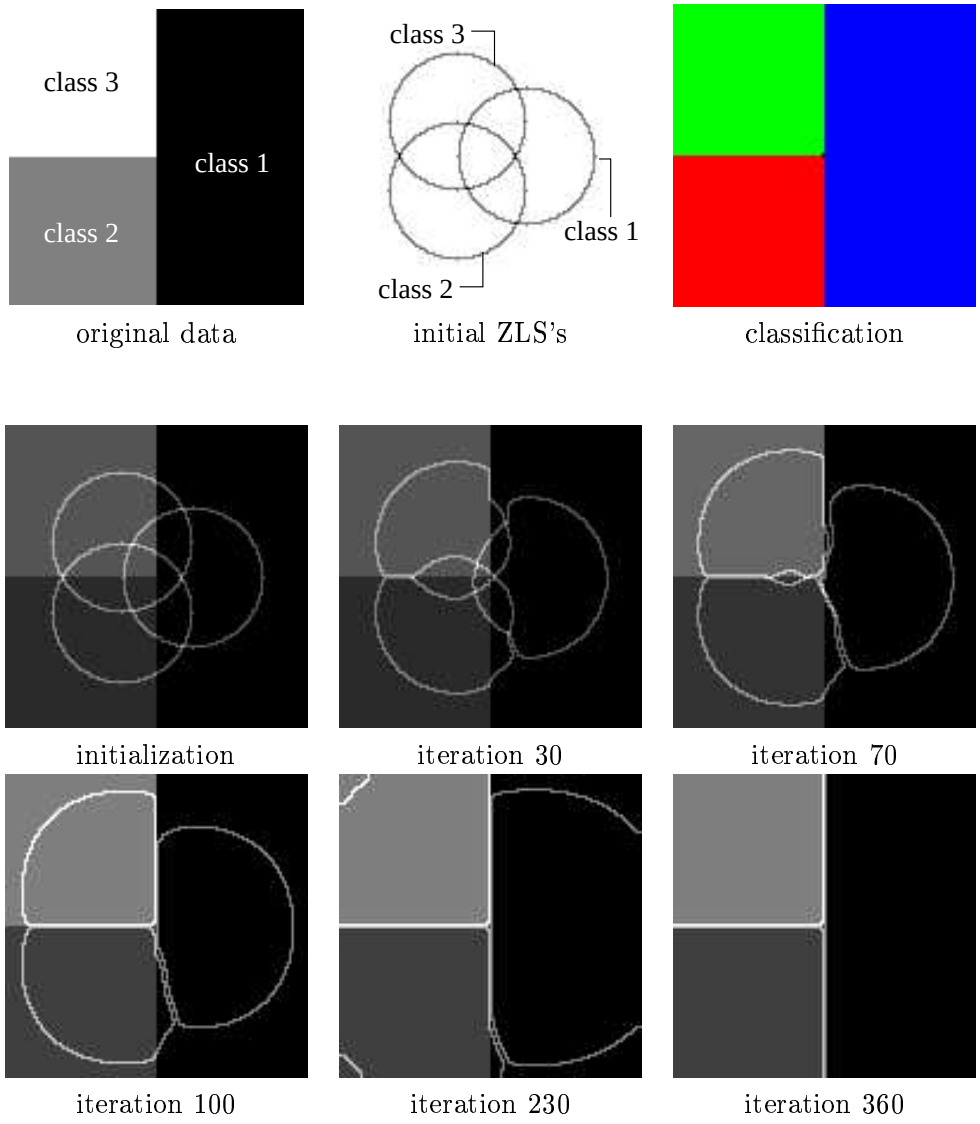

Figure 5: ZLS evolution for three classes ($\mu_1 = 1.0$, $\mu_2 = 2.0$ and $\mu_3 = 3.0$). Parameters are : $\lambda = 5.0$, $dt = 0.2$, and for all i we have $\gamma_i = 1.0$ and $e_i = 2.0$. The classification result on top right handside is a false color image whose black color represents unclassified pixels (pixels of vacuum).

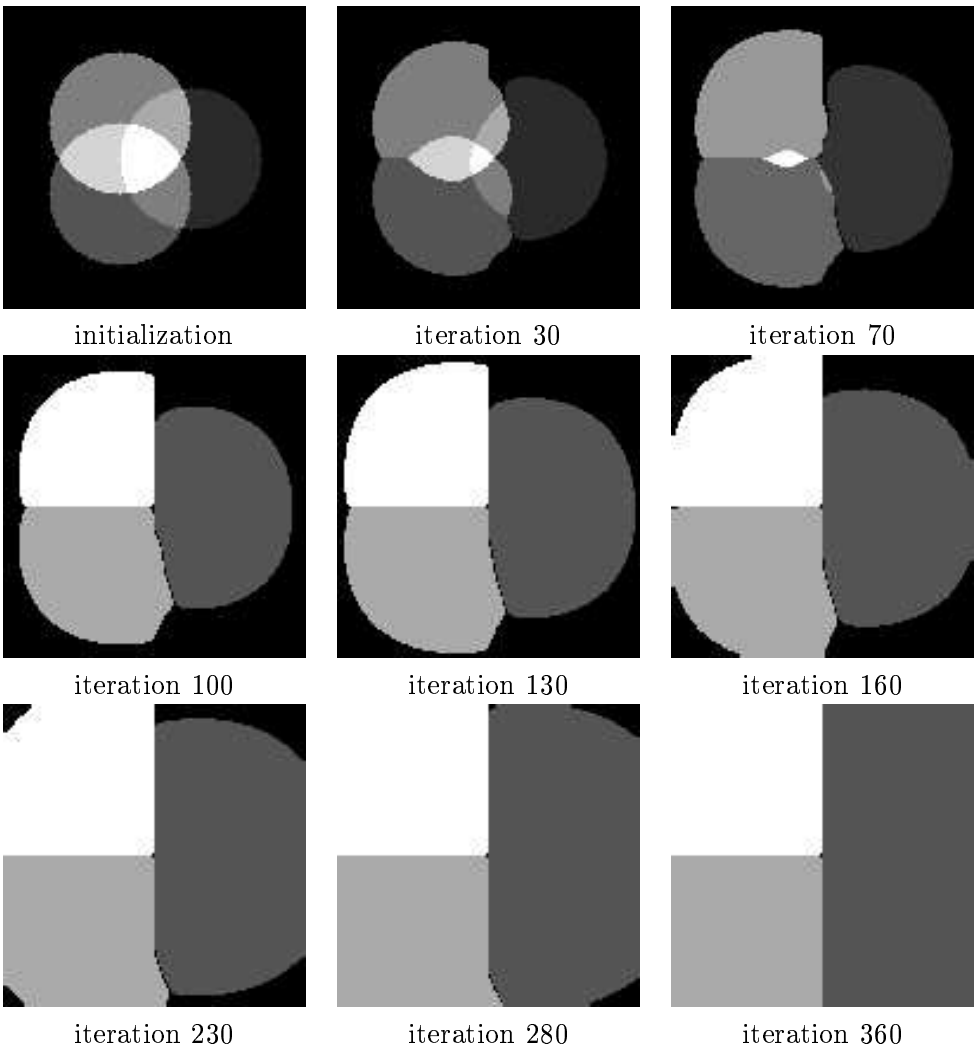

Figure 6: Phase evolution associated to Fig. 5.

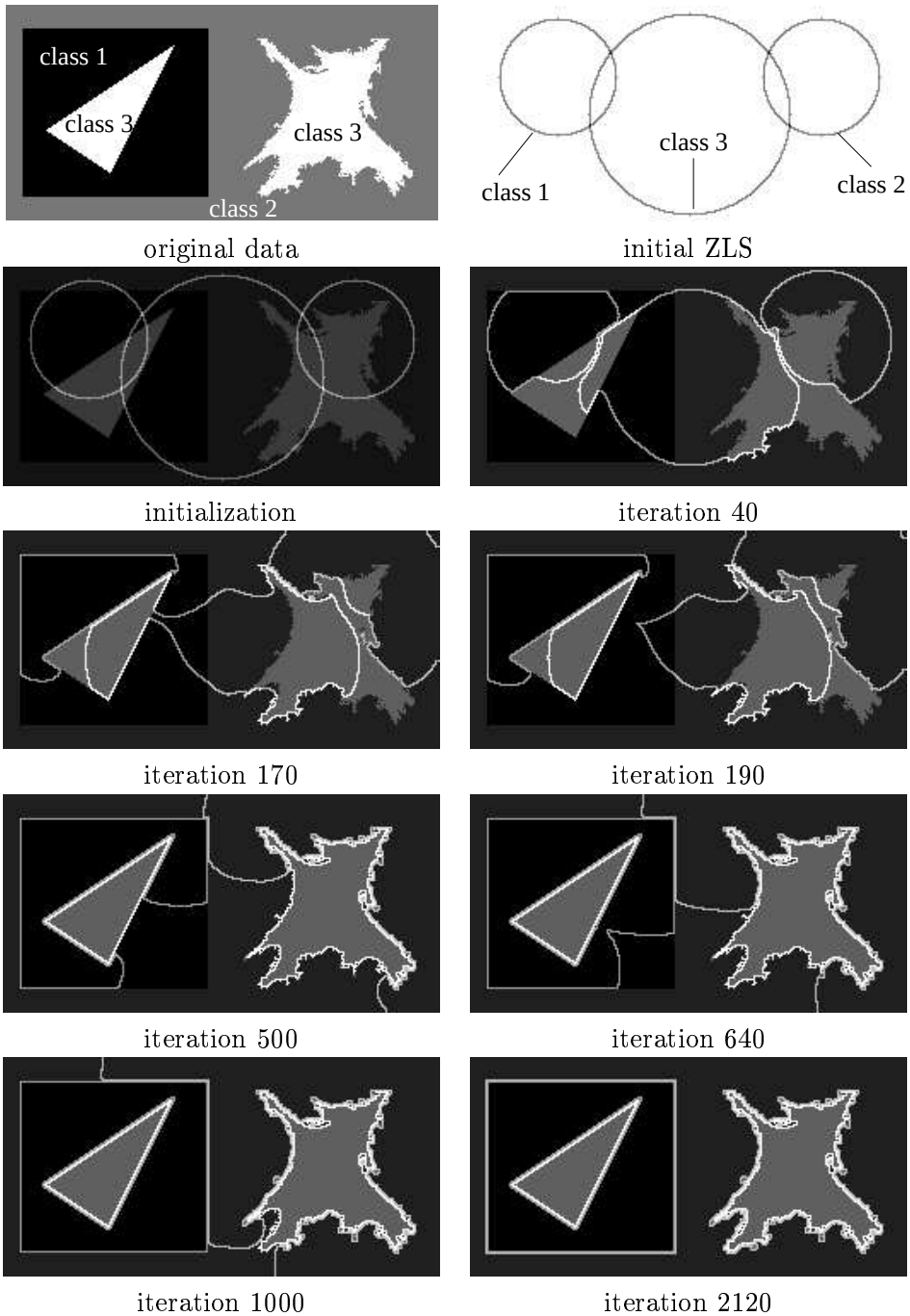

Figure 7: ZLS evolution for three classes ($\mu_1 = 100.0$, $\mu_2 = 128.0$ and $\mu_3 = 160.0$). Parameters are : $\lambda = 5.0$, $dt = 0.2$, and for all i we have $\gamma_i = 0.1$ and $e_i = 0.01$.

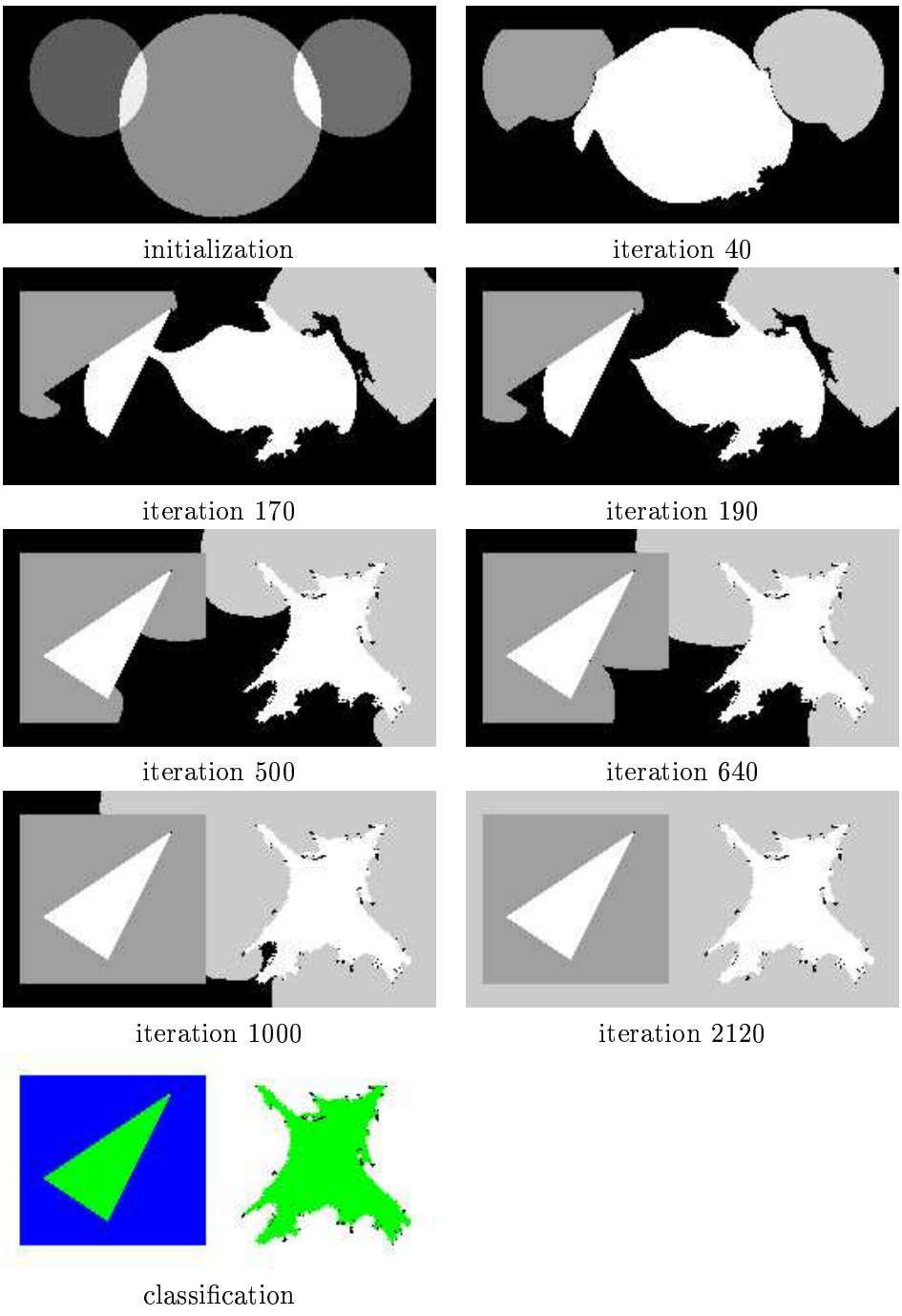

Figure 8: Phase evolution associated to Fig. 7. Last figure is the false color classification result whose black color represents unclassified pixels (pixels of vacuum).

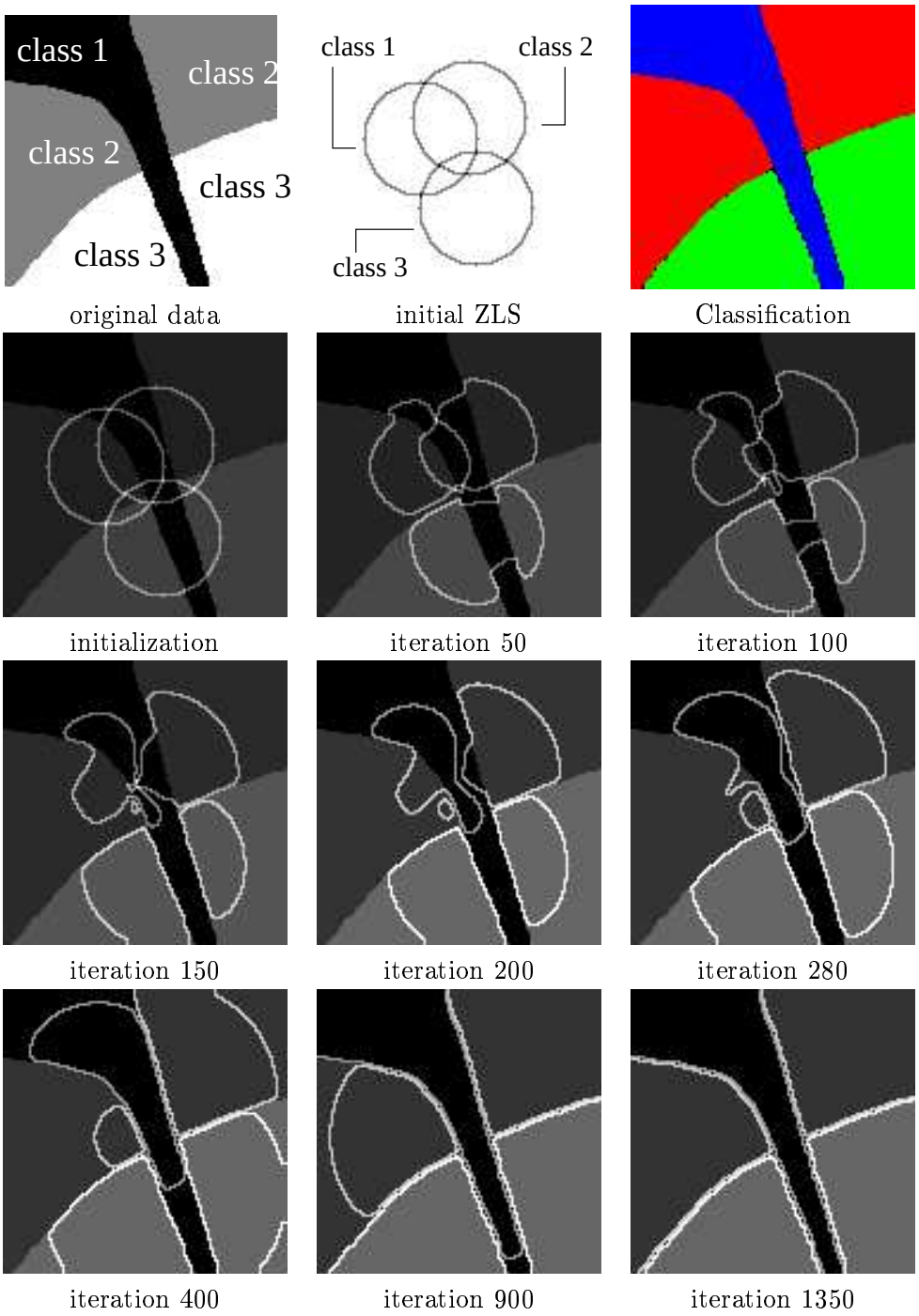

Figure 9: ZLS evolution for three classes ($\mu_1 = 0.0$, $\mu_2 = 1.0$ and $\mu_3 = 2.0$). Parameters are : $\lambda = 2.0$, $dt = 0.2$, and for all i we have $\gamma_i = 0.4$ and $e_i = 2.0$. The false color image on top right handside is the classification result whose black color represents unclassified pixels (pixels of vacuum).

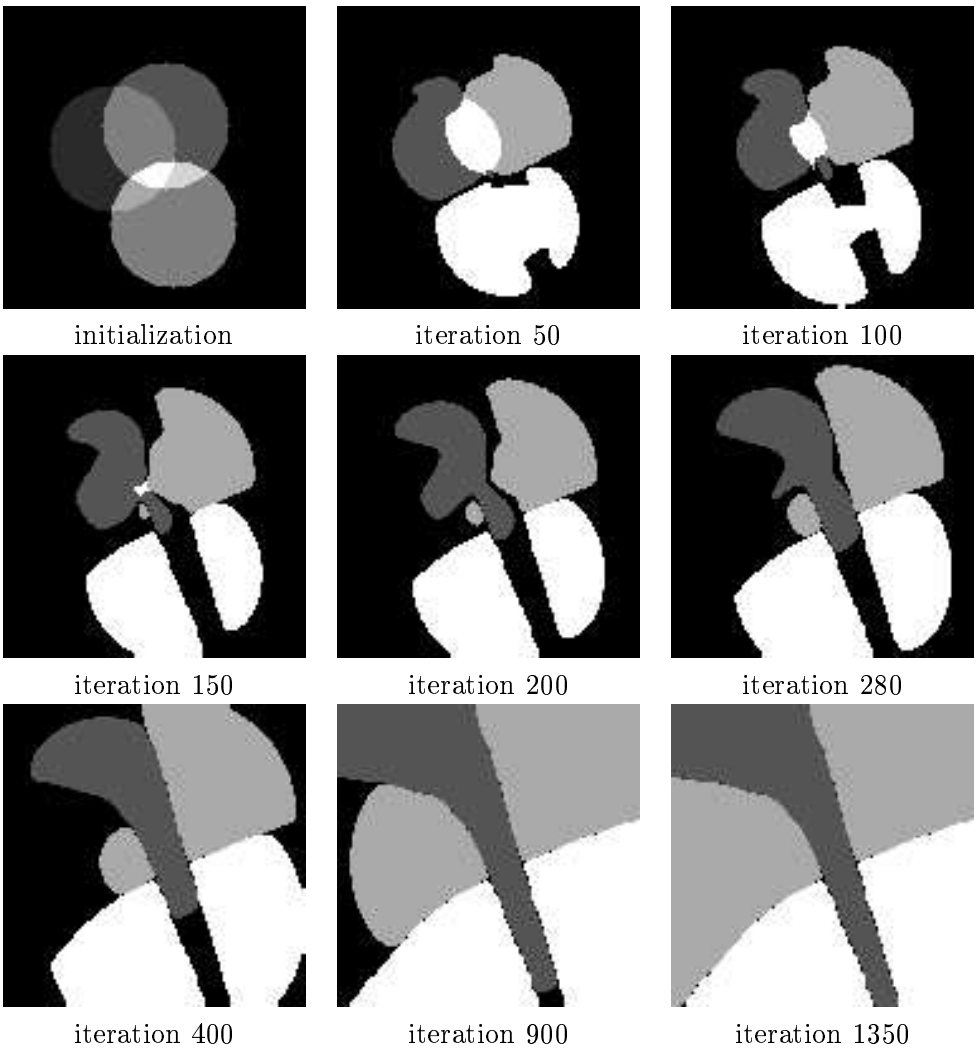

Figure 10: Phase evolution associated to Fig 9.

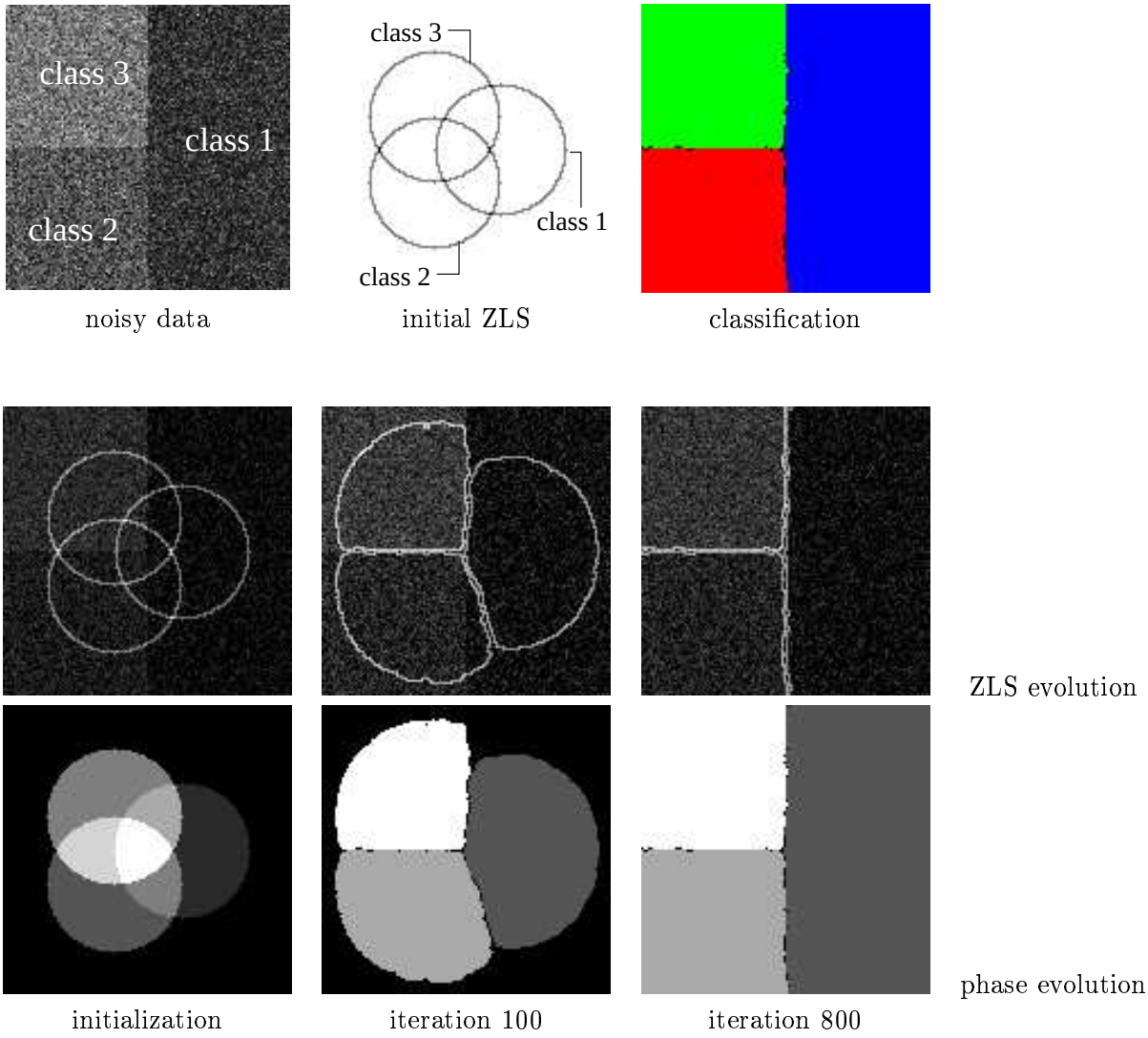

Figure 11: Noisy version (-1.6 dB) of data presented on Fig. 5; ZLS and phase evolution of the Φ_i's for three classes ($\mu_1 = 1.0$, $\mu_2 = 2.0$ and $\mu_3 = 3.0$) . Parameters are : $\lambda = 7.0$, $dt = 0.2$, and for all i we have $\gamma_i = 4.0$ and $e_i = 1.0$. The false color image on top right handside is the classification result whose black color represents unclassified pixels (pixels of vacuum).

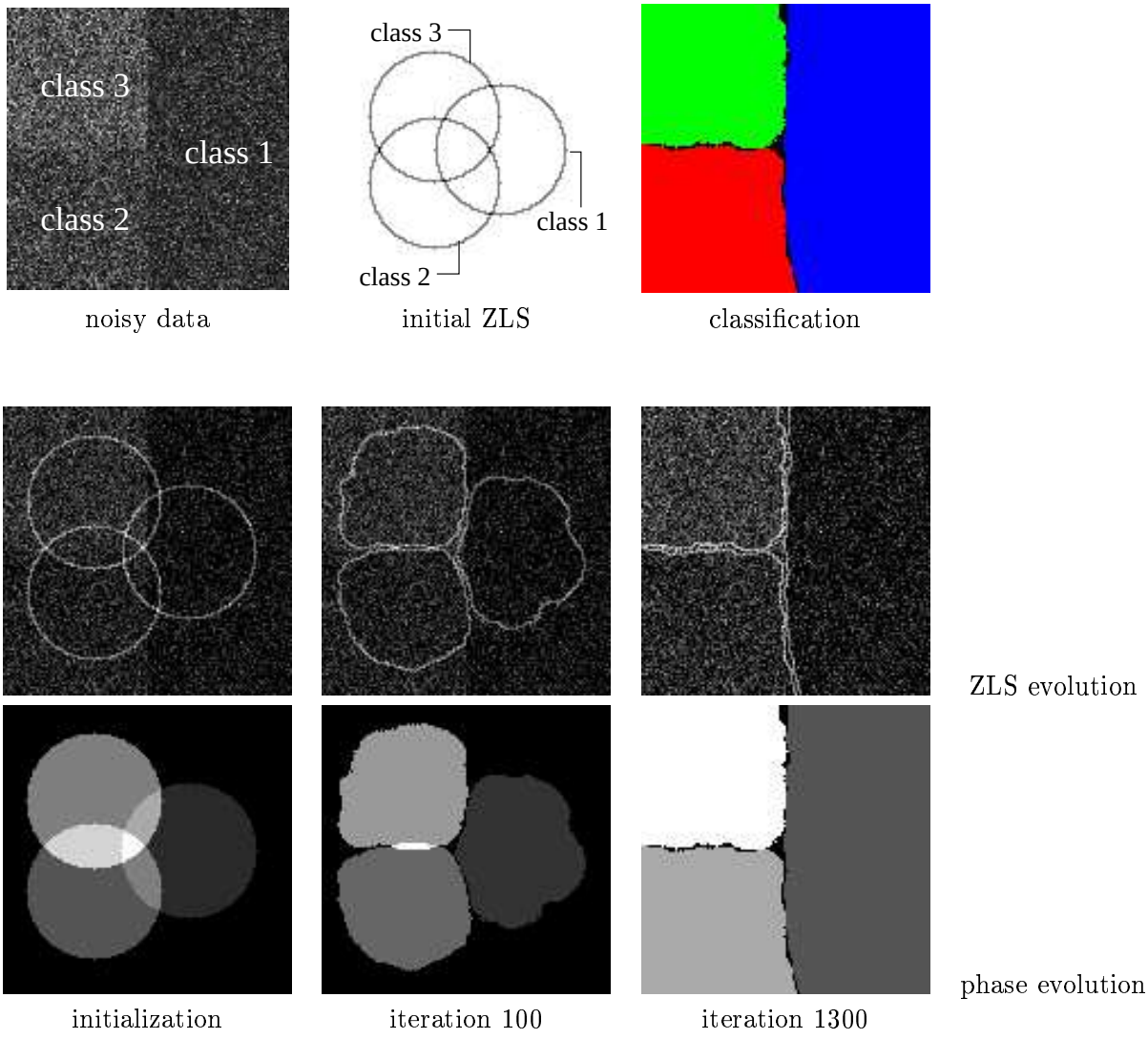

Figure 12: Noisy version (-6.4 dB) of data presented on Fig. 5; ZLS and phase evolution of the Φ_i's for three classes ($\mu_1 = 1.0$, $\mu_2 = 2.0$ and $\mu_3 = 3.0$). Parameters are : $\lambda = 10.0$, $dt = 0.2$, and for all i we have $\gamma_i = 15.0$ and $e_i = 1.0$. The false color image on top right handside is the classification result whose black color represents unclassified pixels (pixels of vacuum).

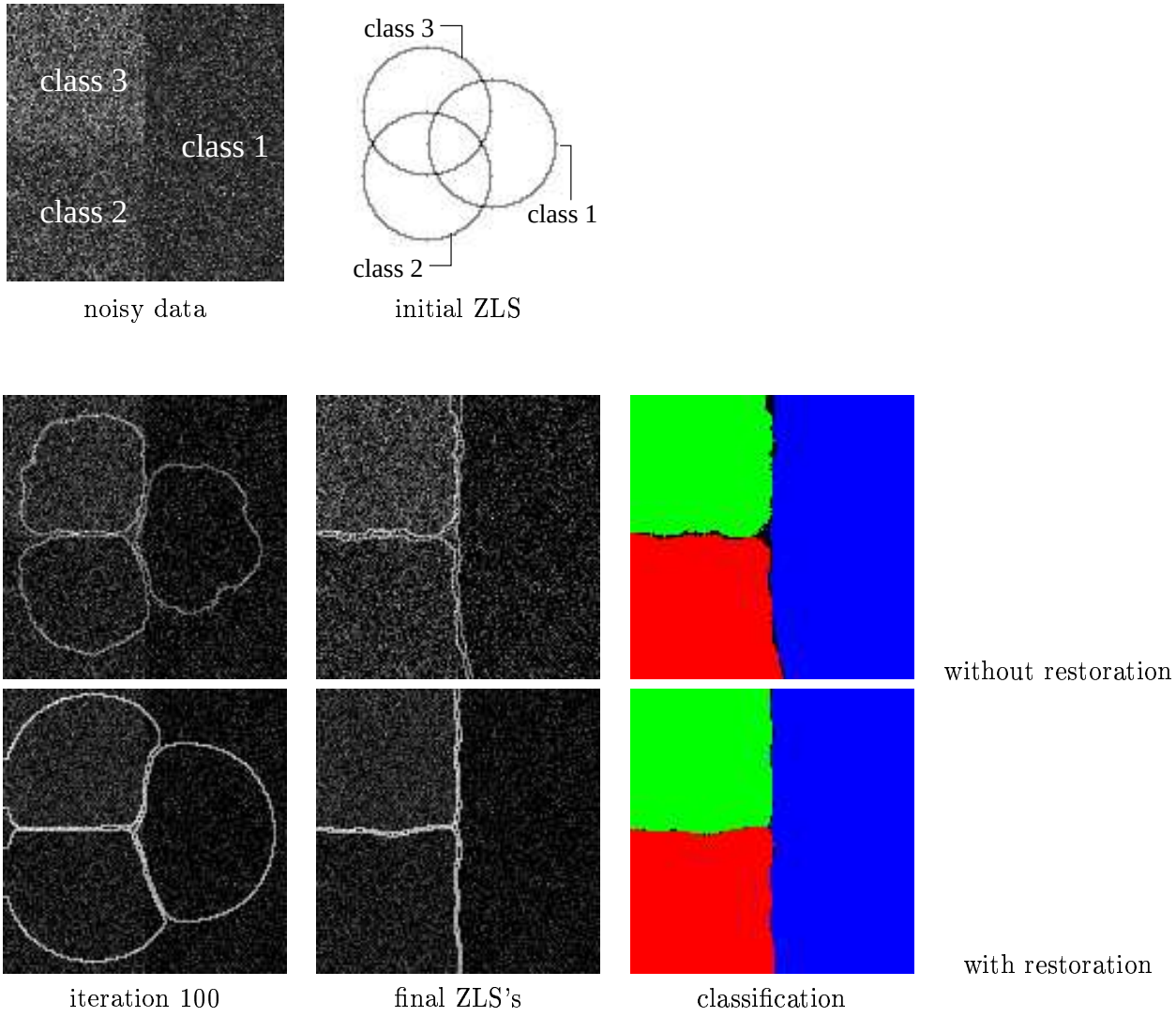

Figure 13: Noisy version (-6.4 dB) of data presented on Fig. 5. Comparison of the results given from the minimization of (16), i.e. without restoration, on the top handside, and from the minimization of (26), i.e with restoration coupled to the classification, on bottom handside. We present two steps of the ZLS's evolution, and the classification results are false color images.

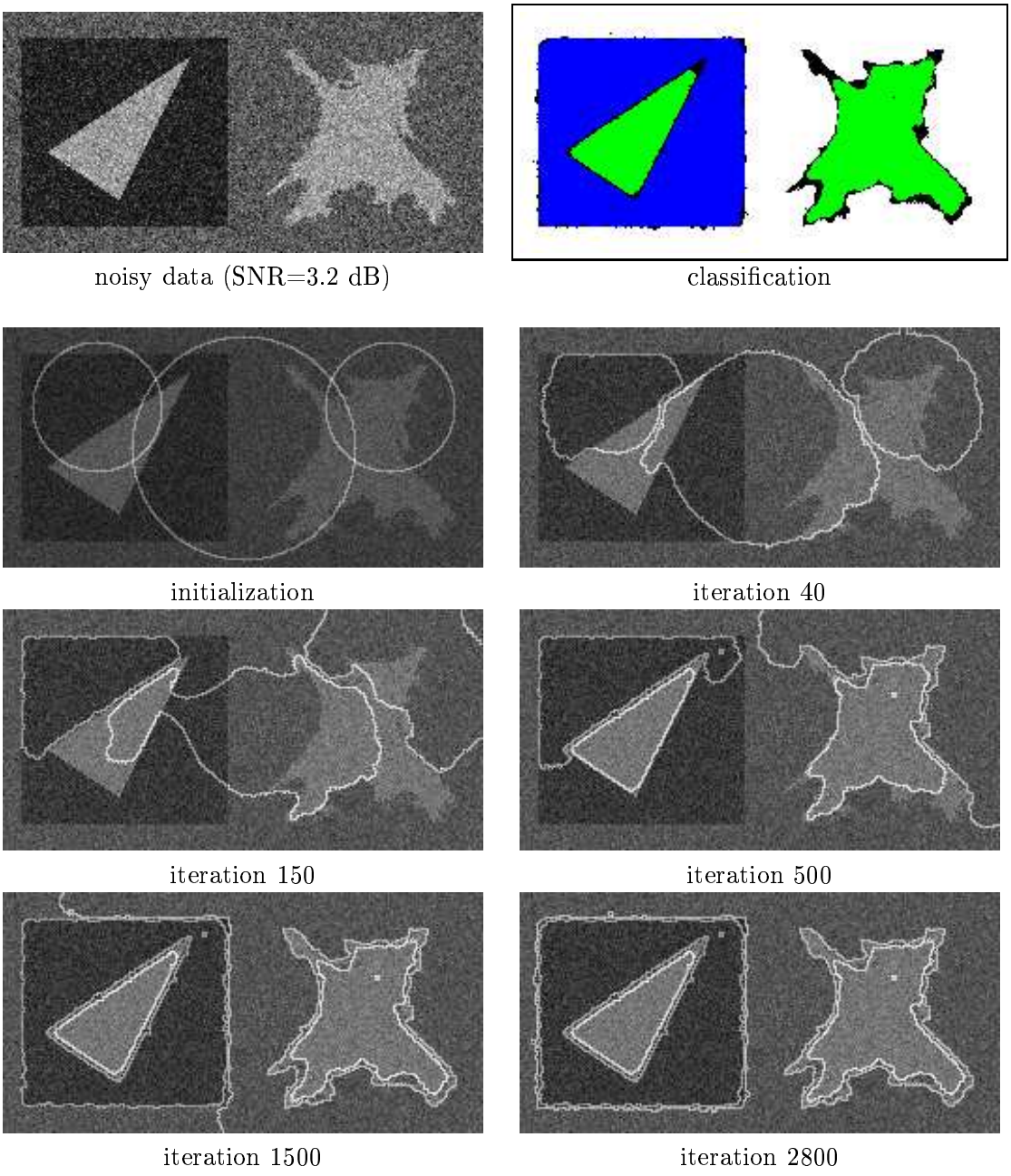

Figure 14: Noisy data : noisy version of data presented on Fig. 7 (SNR=3.2 dB). ZLS evolution for three classes with manual initialization. Parameters are : $\lambda = 5.0$, $dt = 0.2$, and for all i we have $\gamma_i = 0.2$ and $e_i = 0.001$. The false color image on top right handside is the classification result whose black color represents unclassified pixels (pixels of vacuum).

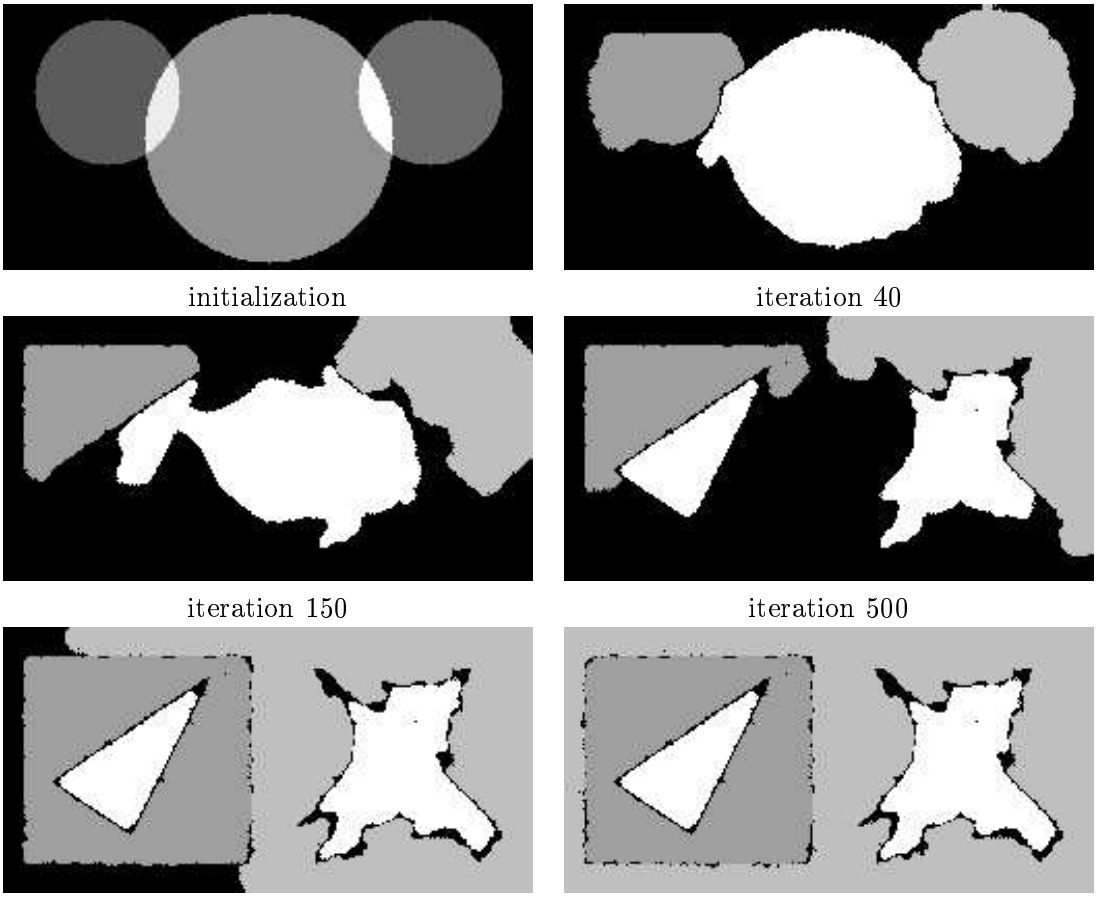

Figure 15: Phase evolution associated to Fig. 14.

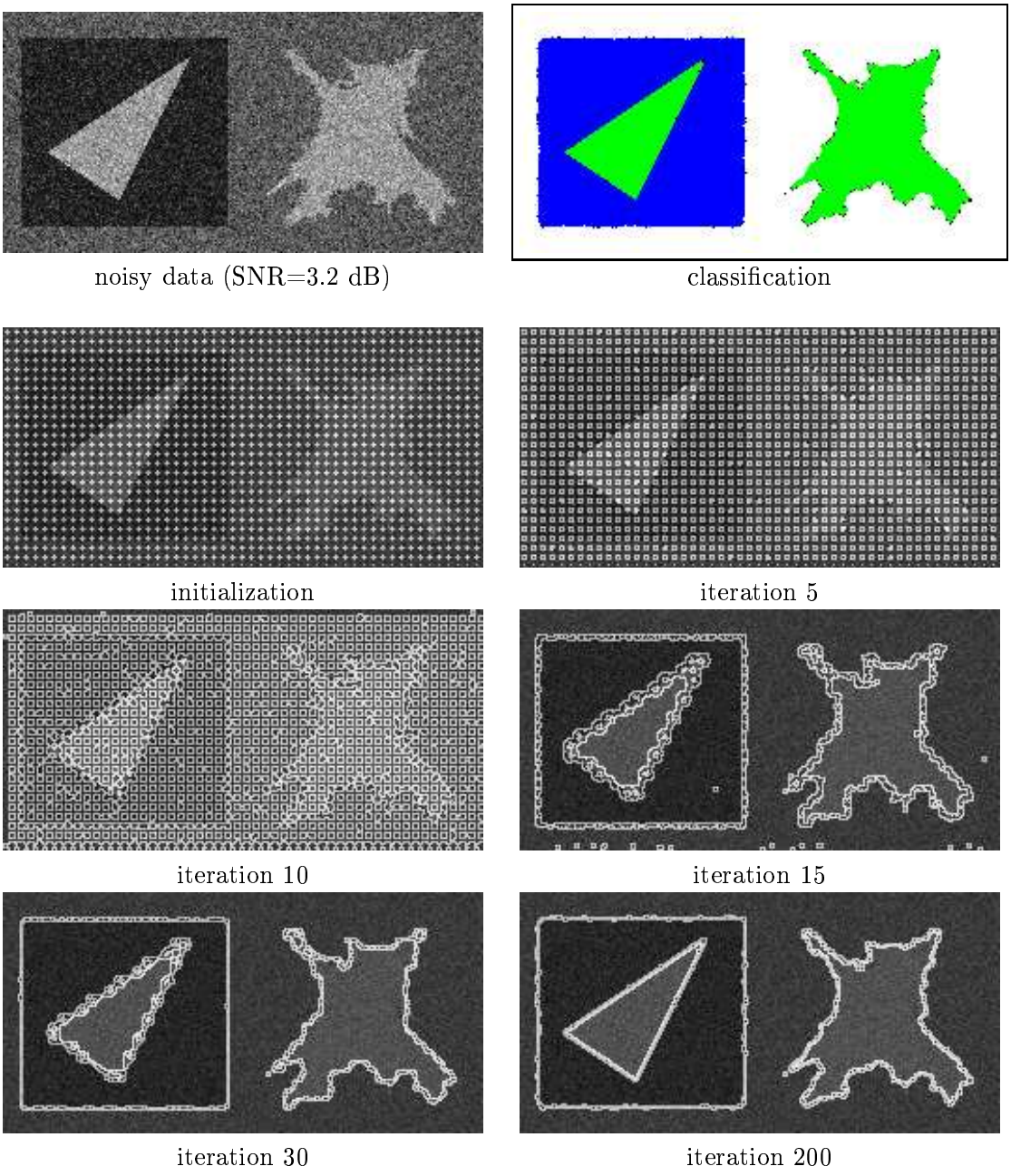

Figure 16: Noisy data : noisy version of data presented on Fig. 7 (SNR=3.2 dB). ZLS evolution for three classes with seed initialization (on windows of size 5×5). Parameters are : $\lambda = 5.0$, $dt = 0.2$, and for all i we have $\gamma_i = 0.2$ and $e_i = 0.001$. The false color image on top right handside is the classification result whose black color represents unclassified pixels (pixels of vacuum).

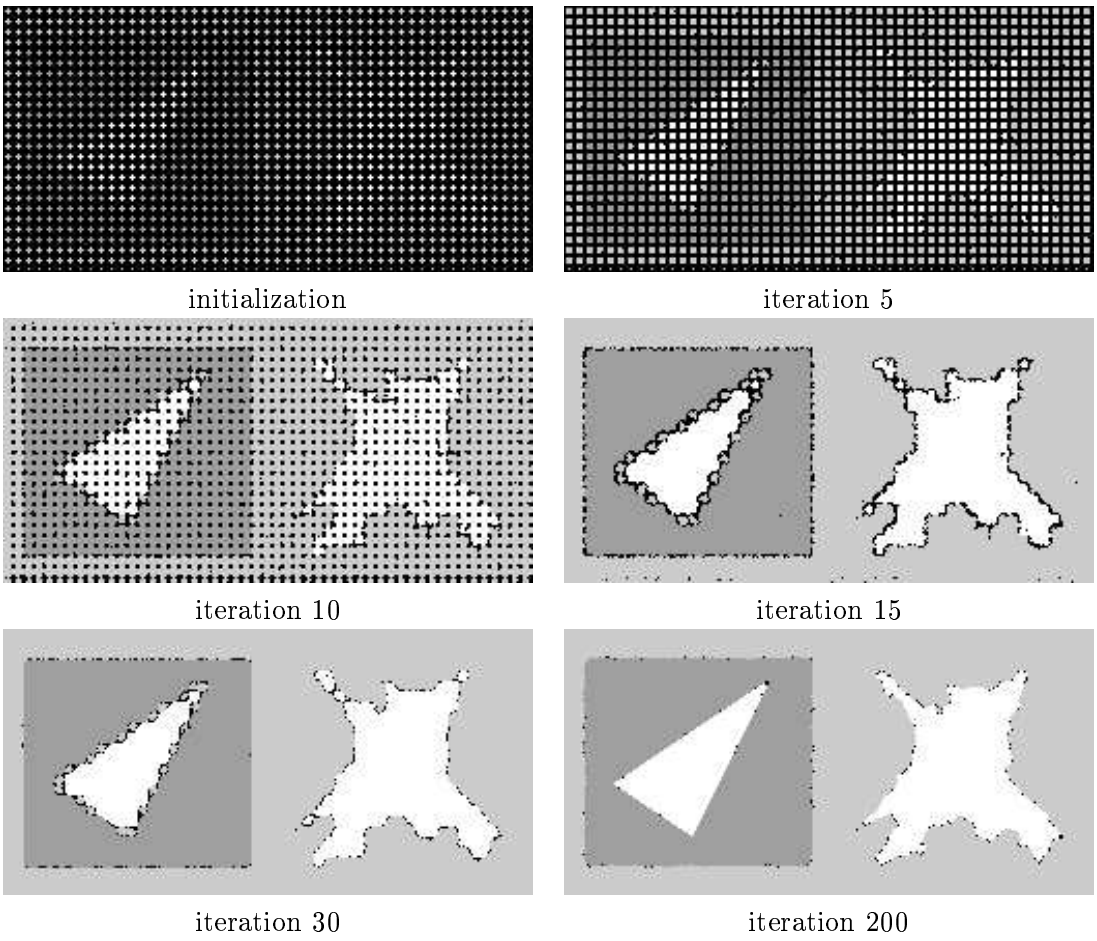

Figure 17: Phase evolution associated to Fig. 16.

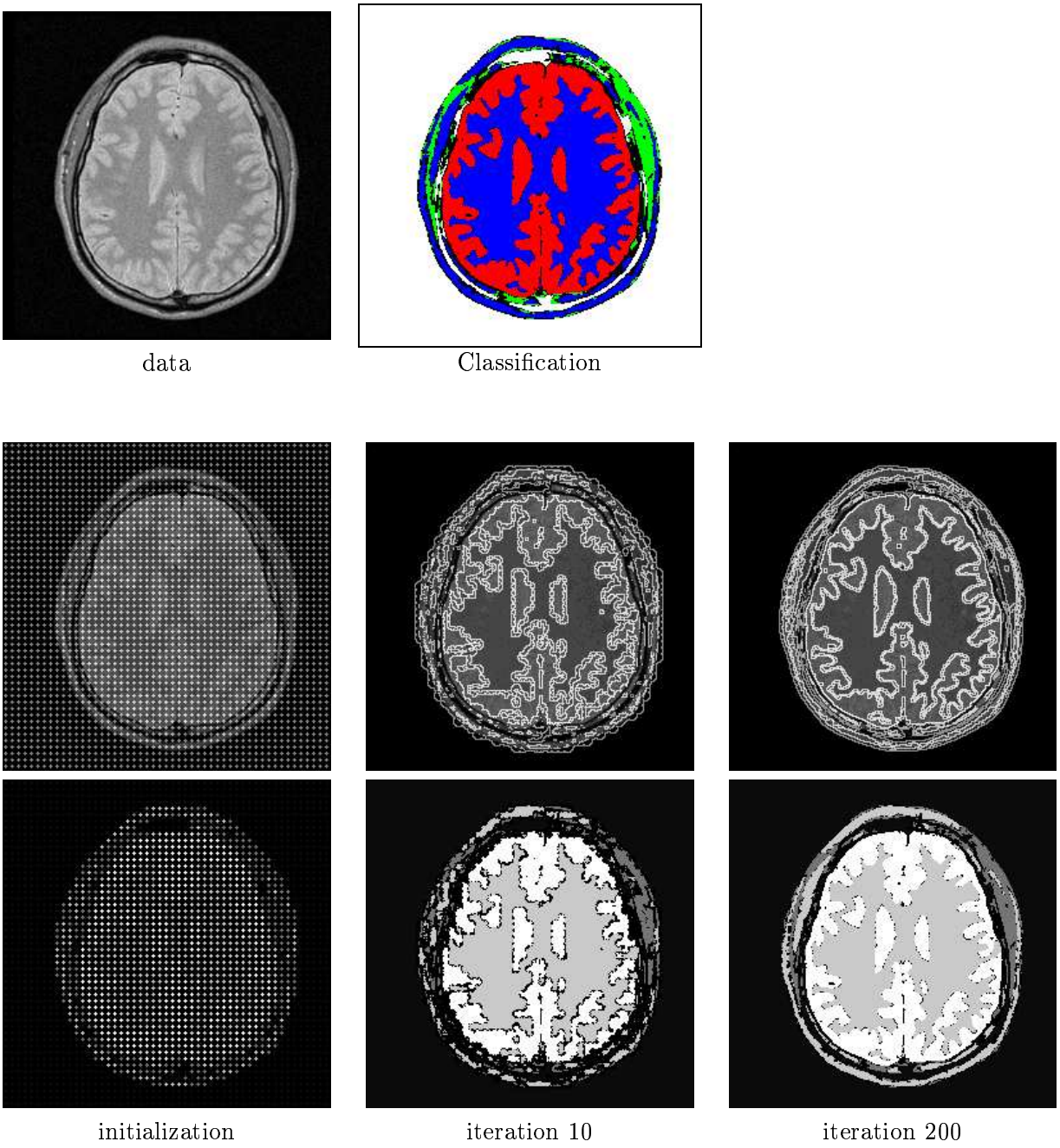

Figure 18: MRI brain data containing 4 classes with seed initialization. We show three steps of the ZLS (top) and phase (bottom) evolutions. The classification result is a false color image whose black color represents unclassified pixels (pixels of vacuum).

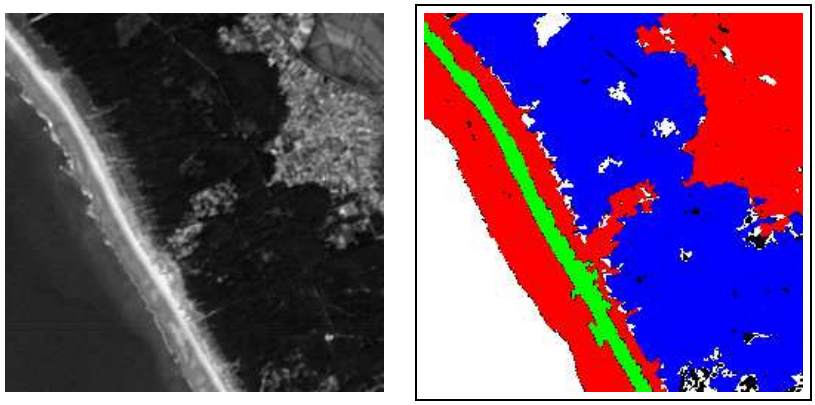

SPOT data classification

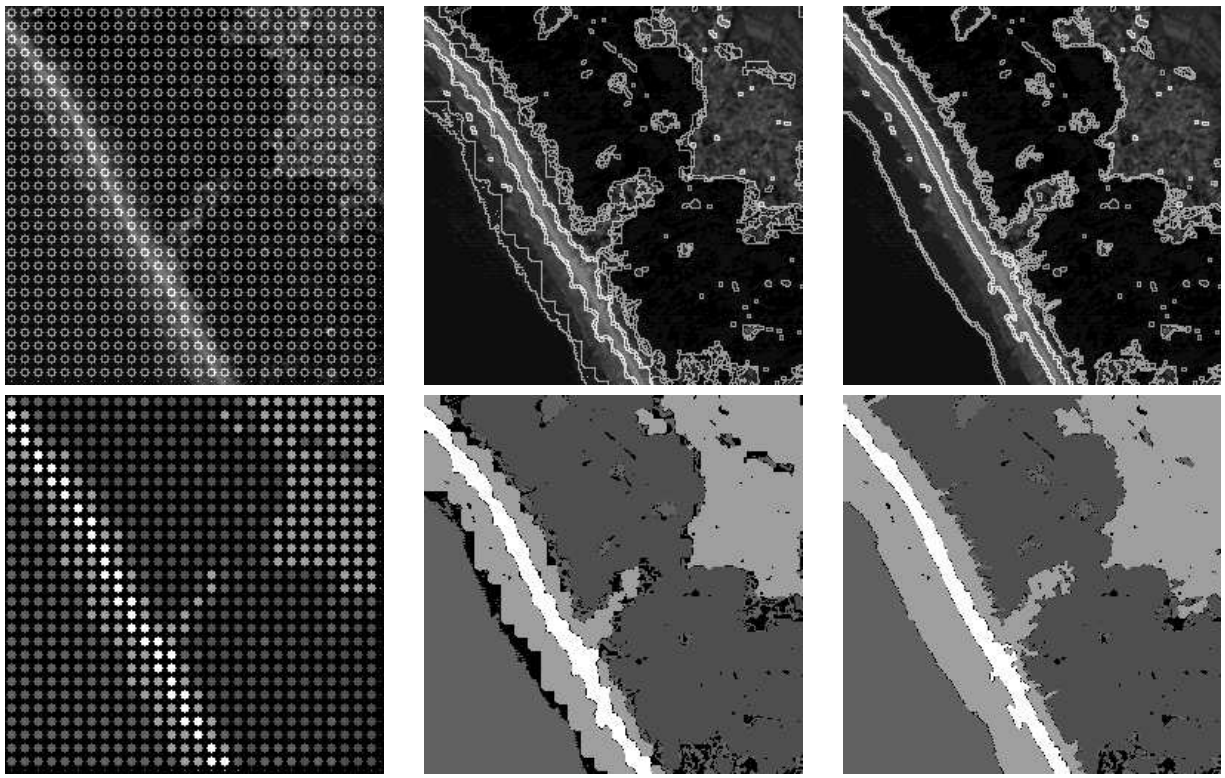

initialization iteration 50 iteration 300

Figure 19: SPOT satellite image containing 4 classes with seed initialization (on windows of size 9×9) : We show three steps of the ZLS (top) and phase (bottom) evolutions. The classification result is a false color image.

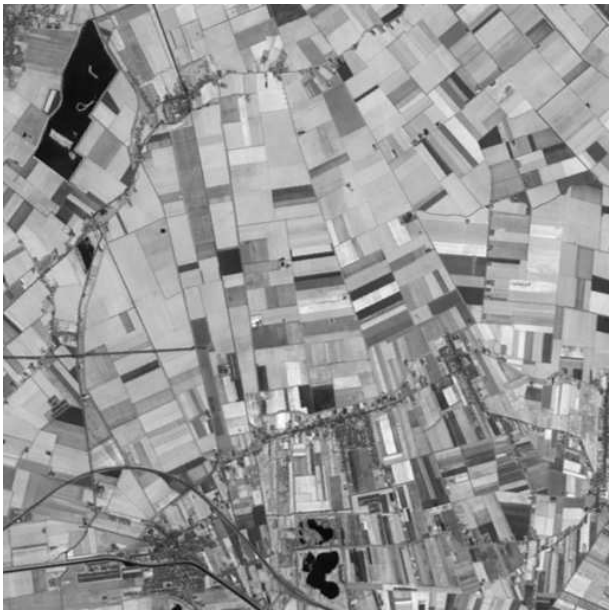

SPOT data

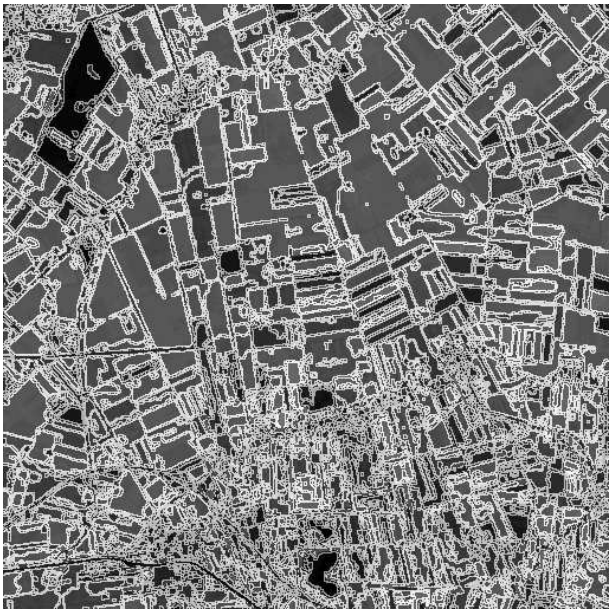

ZLS result

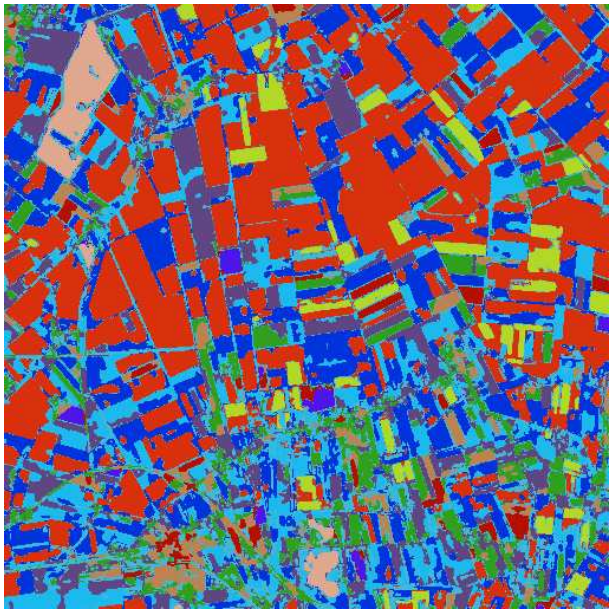

classification result

Figure 20: SPOT satellite image containing 10 classes with seed initialization (windows of size 5×5).

7 Conclusion

We have presented a variational model based on level set formulation for image classification. The level set formulation is a way to represent regions and set of interfaces with a continuous function defined over the whole support of the image. The minimization of the functional leads to a set of coupled PDE's which are considered through a dynamical scheme. Each PDE is guiding a level set function according to internal forces (length minimization), and external ones (data term, no vacuum and no region overlapping). Results on both synthetic and satellite images are given. We also propose a way of introducing a restoration capability in the model. First results are promising, and we will study more precisely this model in future work. Further work will also be conducted to deal with the estimation of the class parameters (unsupervised classification). We also envisage to extend this model to multispectral data (with applications to multiband satellite data and applications to color imaging).

Acknowledgements

We thank Pierre Kornprobst for the synthetic data shown on Fig. 9 and for helpfull comments. We also thank the French Space Agency CNES for providing SPOT satellite images, the Gdr ISIS for original data on Fig. 7, and Dr. Dormont from La Pitié Salpétrière Hospital for providing MRI data.

Appendix

We describe the intermediate calculus to obtain (22) from (16).
From (11), (12) and (15) we can write

$$\begin{aligned} F_\alpha(\Phi_1,...,\Phi_K) &= F_\alpha^{\mathrm{A}}(\Phi_1,...,\Phi_K) + F_\alpha^{\mathrm{B}}(\Phi_1,...,\Phi_K) + F_\alpha^{\mathrm{C}}(\Phi_1,...,\Phi_K) \\ &= \int_\Omega \mathcal{L}_\alpha^a(\Phi_1,...,\Phi_K,\nabla\Phi_1,...,\nabla\Phi_k,x)dx \\ &+ \int_\Omega \mathcal{L}_\alpha^b(\Phi_1,...,\Phi_K,\nabla\Phi_1,...,\nabla\Phi_k,x)dx \\ &+ \int_\Omega \mathcal{L}_\alpha^c(\Phi_1,...,\Phi_K,\nabla\Phi_1,...,\nabla\Phi_k,x)dx \end{aligned}$$

If $(\Phi_1,...,\Phi_K)$ is solution of the minimization of F_α, then necessarily

$$\frac{\partial F_\alpha}{\partial \Phi_i} = 0, \forall i = 1...K$$

and the Euler Lagrange equations for every $i = 1...K$ (with Neumann conditions on $\partial\Omega$) leads to

- $$\begin{aligned} \frac{\partial F_\alpha^{\mathrm{A}}}{\partial \Phi_i} &= \frac{\partial \mathcal{L}_\alpha^a}{\partial \Phi_i} - div\Big(\frac{\partial \mathcal{L}_\alpha^a}{\partial \nabla \Phi_i}\Big) \\ &= \lambda\delta_\alpha(\Phi_i)\Big(\sum_{i=1}^{K} H_\alpha(\Phi_i) - 1\Big) \end{aligned}$$

- $$\begin{aligned} \frac{\partial F_\alpha^{\mathrm{B}}}{\partial \Phi_i} &= \frac{\partial \mathcal{L}_\alpha^b}{\partial \Phi_i} - div\Big(\frac{\partial \mathcal{L}_\alpha^b}{\partial \nabla \Phi_i}\Big) \\ &= \frac{\partial H_\alpha}{\partial \Phi_i}(\Phi_i)\frac{(u_0-\mu_i)^2}{\sigma_i^2} \\ &= \delta_\alpha(\Phi_i)\frac{(u_0-\mu_i)^2}{\sigma_i^2} \end{aligned}$$

- $$\begin{aligned} \frac{\partial F_\alpha^{\mathrm{C}}}{\partial \Phi_i} &= \frac{\partial \mathcal{L}_\alpha^c}{\partial \Phi_i} - div\Big(\frac{\partial \mathcal{L}_\alpha^c}{\partial \nabla \Phi_i}\Big) \\ &= \gamma_i\Big[\delta_\alpha'(\Phi_i)|\nabla\Phi_i| - div\big(\delta_\alpha(\Phi_i)\frac{\nabla\Phi_i}{|\nabla\Phi_i|}\big)\Big] \end{aligned}$$

and if $x = (x_1, x_2) \in \Omega$ we have

$$\begin{aligned} div\big(\delta_\alpha(\Phi_i)\frac{\nabla\Phi_i}{|\nabla\Phi_i|}\big) &= \frac{\partial}{\partial x_1}\big(\delta_\alpha(\Phi_i)\frac{\nabla\Phi_i}{|\nabla\Phi_i|}\big) + \frac{\partial}{\partial x_2}\big(\delta_\alpha(\Phi_i)\frac{\nabla\Phi_i}{|\nabla\Phi_i|}\big) \\ &= \frac{\partial\delta_\alpha}{\partial\Phi_i}(\Phi_i)\frac{\partial\Phi_i}{\partial x_1}\frac{\nabla\Phi_i}{|\nabla\Phi_i|} + \frac{\partial\delta_\alpha}{\partial\Phi_i}(\Phi_i)\frac{\partial\Phi_i}{\partial x_2}\frac{\nabla\Phi_i}{|\nabla\Phi_i|} + \delta_\alpha(\Phi_i)div\big(\frac{\nabla\Phi_i}{|\nabla\Phi_i|}\big) \\ &= \delta'_\alpha(\Phi_i)|\nabla\Phi_i| + \delta_\alpha(\Phi_i)div\big(\frac{\nabla\Phi_i}{|\nabla\Phi_i|}\big) \end{aligned}$$

thus,

$$\frac{\partial F^c_\alpha}{\partial\Phi_i} = -\delta_\alpha(\Phi_i)div\big(\frac{\nabla\Phi_i}{|\nabla\Phi_i|}\big)$$

References

[1] G. Barles, H. M. Soner, and P.E. Souganidis. "Front propagation and phase field theory". *SIAM J. Control and Optimization*, 31:439–479, 1993.

[2] M. Berthod, Z. Kato, S. Yu, and J. Zerubia. "Bayesian image classification using Markov random fields". *Image and Vision Computing*, 14(4):285–293, 1996.

[3] C.A. Bouman and M. Shapiro. "A multiscale random field model for Bayesian image segmentation". *IEEE Trans. on Image Processing*, 3:162–177, March 1994.

[4] V. Caselles, F. Catte, T. Coll, and F. Dibos. "A geometric model for active contours". *Numerische Mathematik*, 66:1–31, 1993.

[5] V. Caselles, R. Kimmel, and G. Sapiro. "Geodesic active contours". *International J. of Computer Vision*, 22(1):61–79, 1997.

[6] P. Charbonnier, L. Blanc-Féraud, G. Aubert, and M. Barlaud. "Deterministic edge-preserving regularization in computed imaging". *IEEE Trans. on Image Processing*, 6(2):298–311, February 1997.

[7] X. Descombes, R. Morris, and J. Zerubia. "Some improvements to Bayesian image segmentation. Part one : modelling. (in french)". *Traitement du Signal*, 14(4):373–382, 1997.

[8] X. Descombes, R. Morris, and J. Zerubia. "Some improvements to Bayesian image segmentation. Part two : classification. (in french)". *Traitement du Signal*, 14(4):383–395, 1997.

[9] L. C. Evans and R. F. Gariepy. *"Measure theory and fine properties of functions"*. CRC Press, 1992.

[10] L.C. Evans and J. Spruck. "Motion of level sets by mean curvature. II". *Trans. of the American Mathematical Society*, 330(1):321–332, 1992.

[11] S. Geman and G. Reynolds. "Constrained restoration and the recovery of discontinuities". *IEEE Trans. on Pattern Analysis and Machine Intelligence*, 14(3):367–383, 1992.

[12] M. Kass, A. Witkin, and D. Terzopoulos. "Snakes : active contour models". *International J. of Computer Vision*, 1:321–331, 1987.

[13] Z. Kato. *"Multiresolution Markovian modeling for computer vision. Application to SPOT image segmentation" (in French and English).* PhD thesis, Université de Nice-Sophia Antipolis, France, 1994.

[14] S. Kichenassamy, A. Kumar, P. Olver, A. Tannenbaum, and A. Yezzi Jr. "Conformal curvature flows : from phase transitions to active vision". *Arch. Rational Mech. Anal.*, 134:275–301, 1996.

[15] S. Lakshmanan and H. Derin. "Simultaneous parameter estimation and segmentation of Gibbs random fields using simulated annealing". *IEEE Trans. on Pattern Analysis and Machine Intelligence*, 11:799–813, August 1989.

[16] R. Malladi, J.A. Sethian, and B.C. Vemuri. "Evolutionary fronts for topology independent shape modeling and recovery". In *Proc. of the 3rd ECCV*, pages 3–13, Stockholm, Sweden, 1994.

[17] B. Manjunath and R. Chellappa. "Unsupervised texture segmentation using Markov random fields models". *IEEE Trans. on Pattern Analysis and Machine Intelligence*, 13:478–482, May 1991.

[18] S. Osher and J.A. Sethian. "Fronts propagating with curvature dependent speed : algorithms based on the Hamilton-Jacobi formulation". *J. of Computational Physics*, 79:12–49, 1988.

[19] N. Paragios and R. Deriche. "Geodesic active regions for texture segmentation". INRIA Research Report RR-3440 (http://www.inria.fr/RRRT/publications-eng.html), June 1998.

[20] T. Pavlidis and Y.-T. Liow. "Integrating region growing and edge detection". In *Proc. of IEEE CVPR*, 1988.

[21] R. Ronfard. "Region-based strategies for active contour models". *International J. of Computer Vision*, 13(2):229–251, 1994.

[22] C. Samson, L. Blanc-Féraud, G. Aubert, and J. Zerubia. "Image classification using a variational approach". INRIA Research Report RR-3523 (http://www.inria.fr/RRRT/publications-eng.html), October 1998.

[23] C. Samson, L. Blanc-Féraud, G. Aubert, and J. Zerubia. "Simultaneous image classification and restoration using a variational approach". In *Proc. of IEEE CVPR*, June 1999.

[24] M. Sussman, P. Smereka, and S. Osher. "A level set approach for computing solutions to incompressible two-phase flow". *J. of Computational Physics*, 114:146–159, 1994.

[25] H-K. Zhao, T. Chan, B. Merriman, and S. Osher. "A variational level set approach to multiphase motion". *J. of Computational Physics*, 127:179–195, 1996.

[26] S. C. Zhu and A. Yuille. "Integrating region growing and edge detection". *IEEE Trans. on Pattern Analysis and Machine Intelligence*, 18(9):884–900, 1996.

Unité de recherche INRIA Sophia Antipolis
2004, route des Lucioles - B.P. 93 - 06902 Sophia Antipolis Cedex (France)

Unité de recherche INRIA Lorraine : Technopôle de Nancy-Brabois - Campus scientifique
615, rue du Jardin Botanique - B.P. 101 - 54602 Villers lès Nancy Cedex (France)
Unité de recherche INRIA Rennes : IRISA, Campus universitaire de Beaulieu - 35042 Rennes Cedex (France)
Unité de recherche INRIA Rhône-Alpes : 655, avenue de l'Europe - 38330 Montbonnot St Martin (France)
Unité de recherche INRIA Rocquencourt : Domaine de Voluceau - Rocquencourt - B.P. 105 - 78153 Le Chesnay Cedex (France)

Éditeur
INRIA - Domaine de Voluceau - Rocquencourt, B.P. 105 - 78153 Le Chesnay Cedex (France)
http://www.inria.fr
ISSN 0249-6399